A comparison of the Iberian and Ebro Basins during the Permian and Triassic, eastern Spain: A quantitative subsidence modelling approach

Henar Vargas [a], Jorge M. Gaspar-Escribano [b], José López-Gómez [c], Jan-Diederik Van Wees [d], Sierd Cloetingh [e], Raúl de La Horra [c], Alfredo Arche [c,*]

[a] Repsol Exploración, S.A. Paseo de la Castellana 280, 28046 Madrid, Spain
[b] E.T.S.I. Topografía, Geodesia y Cartografía, Universidad Politécnica de Madrid, Carretera de Valencia Km. 7, 28031 Madrid, Spain
[c] Instituto de Geología Económica-Departamento de Estratigrafía, CSIC-UCM, Facultad de Geología, Universidad Complutense, 28040 Madrid, Spain
[d] TNO-NITG, Princetonlaan 6, PO Box 80015, 3508 TA Utrecht, The Netherlands
[e] Faculteit der Aardwetenschappen, Vrije Universiteit, De Boelelaan 1085, 1081 HV Amsterdam, The Netherlands

Keywords:
Extensional basins
Backstripping
Forward modeling
Subsidence analysis

ABSTRACT

The Permian–Triassic sediments of the Iberian Plate are a well studied case of classical Buntsandstein–Muschelkalk–Keuper facies, with good sedimentological interpretations and precise datings based on pollen and spore assemblages, ammonoids and foraminifera. Synrift–postrift cycles are recorded in these facies, but there are only a few studies of quantitative subsidence analysis (backstripping method) and only a previous one using forward modelling for the quantification of synrift–postrift phases of this period.

Here we present the results obtained by the quantitative analysis of fourteen field sections and oil-well electric log records in the Iberian and Ebro Basins, Spain. Backstripping analysis showed five synrift phases of 1 to 3 million years duration followed by postrift periods for the Permian–Triassic interval. The duration, however, shows lateral variations and some of them are absent in the Ebro Basin. The forward modelling analysis, assuming local isostatic compensation, has been applied to each observation point using one-layer and two-layer lithospheric configurations. The second one shows a better fit between observation and model prediction in a systematic way, so a two layer configuration is assumed for the sedimentary basin filling analysis. Lithospheric stretching factors β and δ obtained in the forward modelling analysis are never higher than 1.2, but sometimes $\beta < 1$ and simultaneously $\delta > 1$ in the same section. If surficial extension is compensated by deep compression either at the roots of the rift basins or in far-away zones is not yet clear, but this anomaly can be explained using a simple shear extensional model for the Iberian and Ebro basins.

1. Introduction

The present-day Iberian, Catalan and Pyrenean Ranges, and the Ebro Basin (Fig. 1), situated in the northeastern Iberian Plate, are the geomorphic expression of basin inversion, thrusting and foreland basin creation during the Cenozoic Alpine compressional events (Vegas and Banda, 1982) in Central and Northern Iberian Peninsula. The three ranges had similar multiple extensional phases of tectonic evolution during Permian and Triassic times. The Iberian Basin originated during the Early Permian as isolated assymetric half-grabens, and developed towards a classic, symmetrical graben during the Early Triassic (Arche and López-Gómez, 1996). Most of the late Permian–early Mesozoic rifting sediments in the Ebro Basin are covered by Cenozoic sediments in the present Ebro Basin or southern foreland basin of the Pyrenees. Core and electric well logs studies (Jurado, 1989; Salvany, 1990) and geophysical data (ECORS Pyrenees Team, 1988; Choukroune, 1989; Salas et al., 2001) show a clearly subdivided basin marked by highs and troughs with different sedimentary characteristics, similar to the Iberian Basin. The Catalan Basin, isolated during Late Permian times from the rest of the Iberian Peninsula by the Lérida, Montalbán–Oropesa and North Catalan Highs, at the north, west and south respectively, and connected at the southwest corner during the Early Triassic with the other basins, also evolved as half-grabens with contrasting sedimentary characteristics (Calvet and Marzo, 1994) (Fig. 1A, 2A), and in consequence, marked differences in the sedimentary record of Permian and Triassic age.

The study of the Ebro and Iberian Basins subsidence during the Permian and Triassic times is the main focus of this paper. Earlier work have shown the subsidence style in the Ebro Basin (Desegaulx and Moretti, 1988; Zoetemeijer et al., 1990; Gaspar-Escribano et al., 2001) and the Iberian Basin (Álvaro, 1987; Arche and López-Gómez, 1999a; Salas and Casas, 1993; Van Wees and Stephenson, 1995; Van Wees et al., 1998). However, none of these studies correlated the subsidence history of both basins during the Permian and Triassic. This period of time corresponds to the beginning of the break-up of Pangea and the

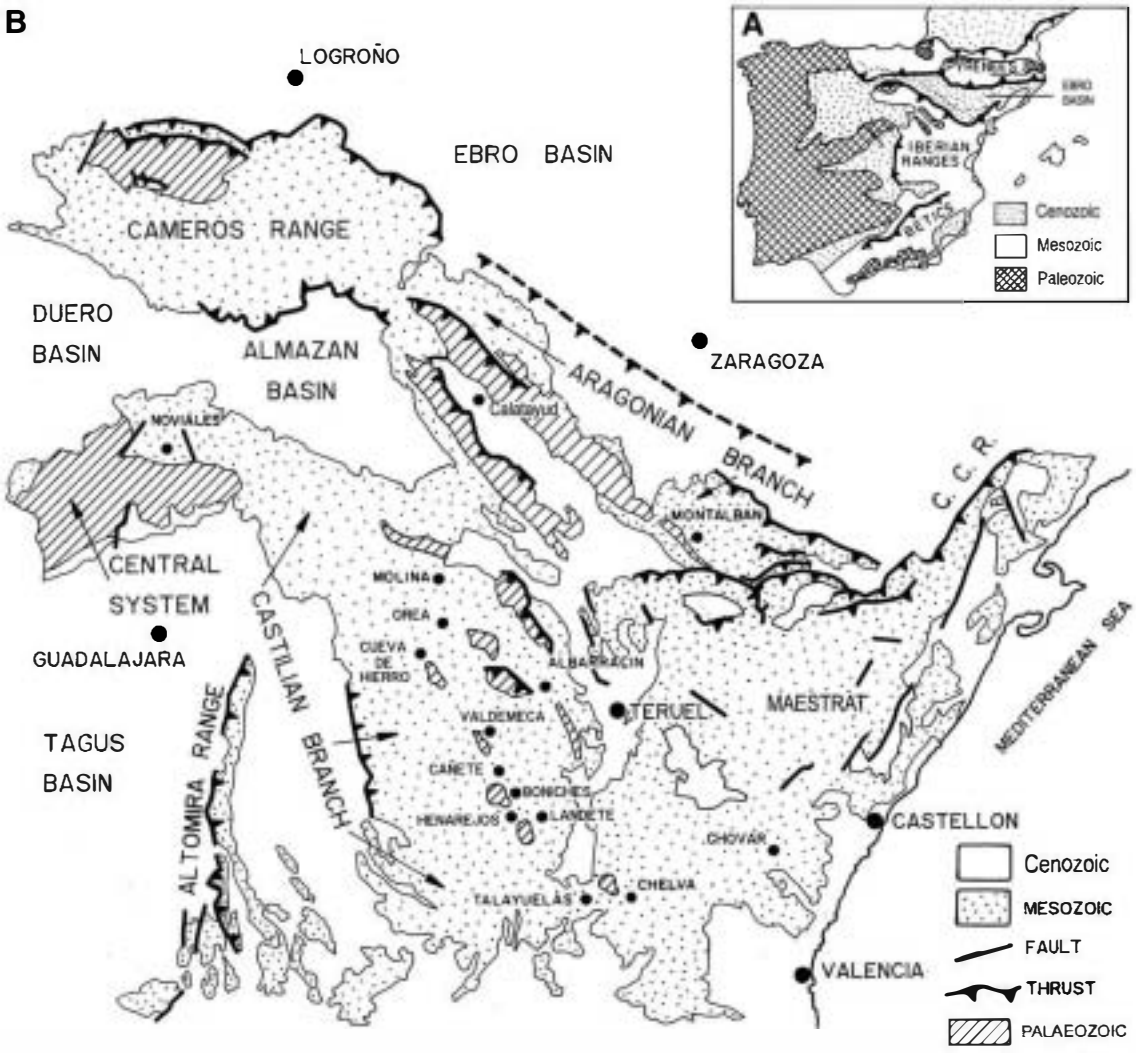

Fig. 1. A — Geological map of the Iberian Peninsula showing the present-day basins, ranges and major Alpine thrust fronts. B — the study area and its more relevant structures.

progressive advance of the Tethys Sea to the west and the different phases of this evolution are poorly known in Iberia. This study will show that, although the evolution was similar in both basins during their early stages, the Ebro and Iberian Basins had different subsidence evolutions.

Previous quantitative studies in both basins have shed much light on the subsidence histories, but were limited in the stratigraphic resolution or were restricted in the number of stretching phases. In this paper we have tried to resolve these problems first in each basin and finally establishing a comparison between them. For this purpose, we first use the backstripping technique on six composed surface sections and eight wells to obtain the tectonic subsidence curves, and the forward modelling technique to obtain the stretching factors.

The modelling is based on a precise program that allows for infinite extensional phases, not for a limited number as used in previous studies, improving the resolution of the analysis. The forward modelling method was used in Van Wees et al. (1998), but improved stratigraphic data used in this paper and the possibility of using one and two-layer extensional modelling also improve on the results available up to now.

The subsidence analysis and forward modelling allows to quantitatively analyse the spatial and temporal variations of predicted crustal and subcrustal stretching values. From this perspective we are able to unravel more about the tectonic processes driving Permian and Mesozoic basin formation in the Ebro and Iberian basins. In particular, we aim to discuss the predictions of forward modelling in the framework of observations on fault morphology and a number of other tectonic processes controlling the evolution of particular sectors of each basin (Leeder and Gawthorpe, 1987; Gibbs, 1990; Kooi et al., 1992; van Wees and Cloetingh, 1994; Gawthorpe and Leeder, 2000; Leeder et al., 2002; Young et al., 2002).

2. Geological framework

The present structure of the NE Iberian Plate is the result of the convergence between the European, Iberian and African plates and the sea-floor spreading episode during the Late Oligocene–Miocene responsible for the opening of the Gulf of Valencia–Gulf of Lyons and eastward migration of the Balearic, Corsica and Sardinia blocks and the creation of the Pyrenean, Iberian and Betic compression orogens. Convergence occurred in two stages (Srivastava et al., 1990; Roest and Srivastava, 1991; Gueguen et al., 1998; Roca et al., 2004): the first one, during Late Cretaceous–Middle Oligocene, (between Eurasia and Iberia), and the second one during Late Oligocene–Early Miocene (between the Iberian and African plates). Extensional phases took place from the Late Miocene onwards.

The Cenozoic Ebro Basin is the present southern foreland basin of the Pyrenees, originated during in the Pyrenean orogeny caused by the collision between Europe and Iberia in Late Paleogene–Earlt Miocene times (Puigdefábregas et al., 1986; Vergés et al., 2002). This foreland basin phase was preceded by tectono-sedimentary phases that created an intracratonic rift basin: a late Paleozoic–early Mesozoic

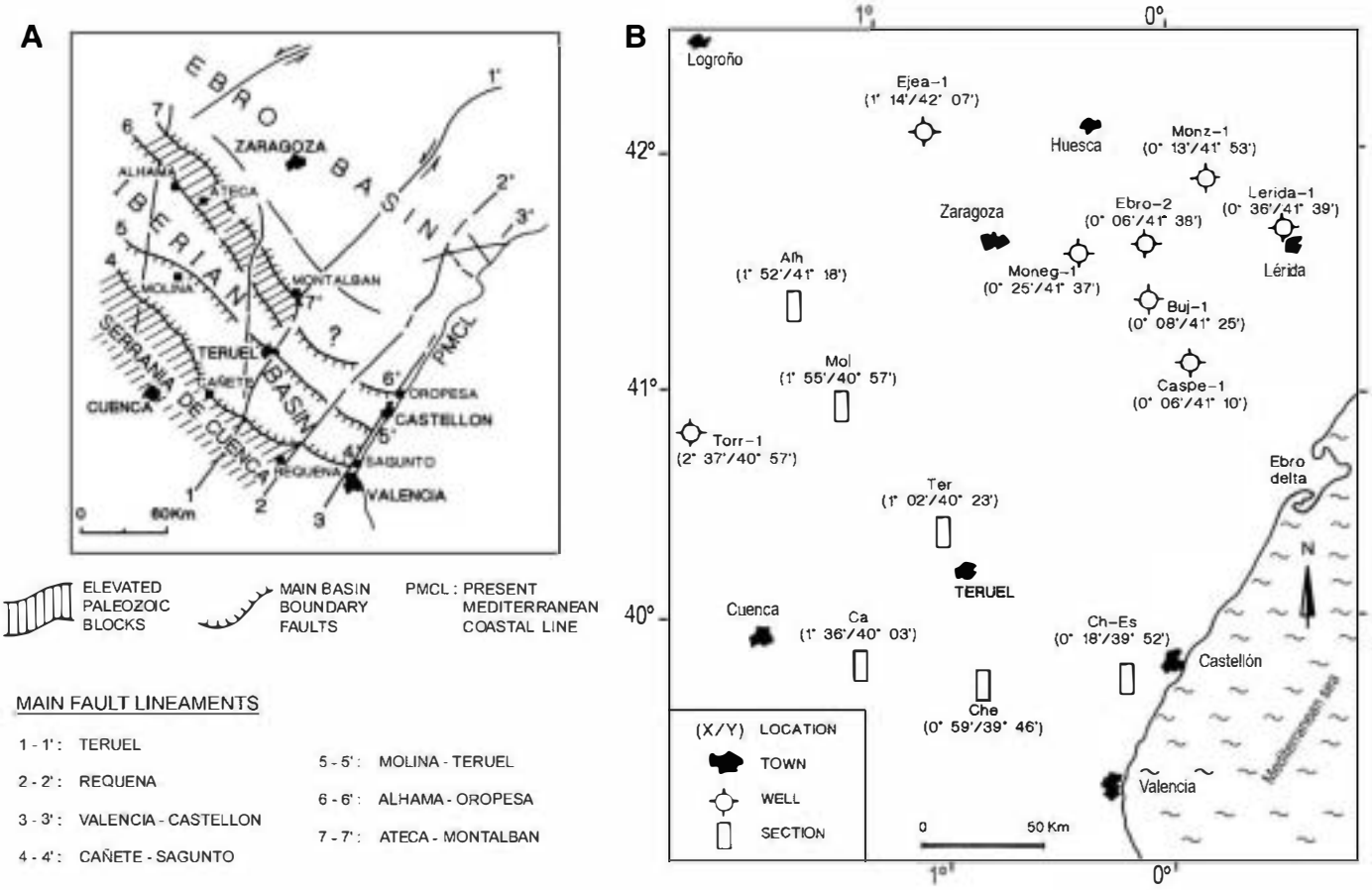

Fig. 2. A — tectonic sketch map and main locations of the study area. B — locations of the studied sections and wells: Torremocha-1 (Torr-1), Molina de Aragón (Mol), Alhama (Alh), Cañete (Ca), Teruel (Ter), Chelva (Che), Chovar-Eslida (Ch-Es), Ejea-1, Monegrillo-1 (Moneg-1), Bujaraloz-1 (Buj-1), Ebro-2, Caspe-1, Manzón-1 (Monz-1), Lérida-1.

rifting, an Early–Middle Cretaceous platform development and a Middle Cretaceous strike-slip tectonic phase (Puigdefábregas et al., 1986). The Ebro Basin is now triangular in shape, bounded to the north by the Pyrenean Chain, to the northeast by the Catalan Coastal Range and to the south by the Iberian Ranges (Fig. 1A). The depocentres of the Ebro Basin migrated from north to south during the Late Paleocene–Early Miocene thrusting episodes (Riba et al., 1983) which shortened in the basin by about 100 km (Roure et al., 1989), and up to 165 km according to Muñoz (1992).

The Iberian Ranges are an intraplate chain bounded by the Central System and the Tajo Basin to the west, the Catalan Coastal Ranges to the northeast and the Cenozoic Ebro Basin to the north (Fig. 1). Its present configuration, with two Paleozoic–Mesozoic lineaments (Castilian and Aragonese branches) separated by the Cenozoic Calatayud–Teruel basin, was formed by the Paleogene–Miocene inversion of an intracontinental NW–SE Mesozoic rift system related to some NW–SE extensive basins (Maestrat and Cameros Basins; Álvaro et al., 1979; Guimerá and Álvaro, 1990; Salas and Casas, 1993).

The Permo–Triassic Iberian Basin is limited by three main NW–SE boundary fault systems: the Cañete–Sagunto (or Serranía de Cuenca), the Molina–Teruel and the Alhama–Oropesa, and the Ateca–Montalbán–Maestrazgo fault systems (Arche and López-Gómez, 1996, 1999a) (Fig. 2A). These fault systems, trending NW–SE and consisting of normal, listric faults, are related to the Hercynian tectonic structures, very active since Late Carboniferous–Early Permian times and controlled the shape and location of the Permian–Triassic infilling of the Iberian Basin (Arche and López-Gómez, 1996; Van Wees et al., 1998) and the later inversion tectonics during the Cenozoic compressive period (Arche and López-Gómez, 1996). A subordinate system of NNE–SSW fault systems was active from Early Permian to Middle Triassic times, the Teruel, Requena and Valencia–Castellón systems, controlling different extensional rates and sedimentation domains, in particular during the Anisian in the eastern part of the Iberian Basin. The northern part of the Ateca–Montalbán–Maestrazgo Fault System corresponds with the southern Ebro Basin boundary (Fig. 2A).

Extension in continental plates along shallow listric normal faults that flat out at a depth of 12–15 Km, in the brittle-ductile transition zone in the continental crust, are very frequent as documented by Gibbs (1984, 1987), Wernicke and Tilke (1989) and Morley (1999), among others. The possible propagation in depth in an ramp-and-flat staircase fault model across the lithosphere and even the upper mantle is a possibility not to be discarded in the Iberian Plate.

The Permo–Triassic Ebro Basin was bounded to the SW by a Paleozoic high, the Soria–Ateca–Montalbán high, to the NE by the Lérida and North Catalan Paleozoic Highs, and to the N by an ill-defined Pyrenean High. These structures of clear tectonic origin were progressively drowned by successive transgressive pulses of the Tethys Sea during the Middle–Upper Triassic (López-Gómez et al., 1998).

There were three main phases of deposition in the Iberian Basin during the Permian and Triassic: an initial short-lived rifting phase in the Autunian (Early Permian) corresponding to the formation of small local basins (Van Wees et al., 1998), a second rifting phase (Late Permian–Early Triassic) related to the first stage of Iberian and Ebro basin formation as a response to lithospheric stretching, trending NW–SE (main direction of Hercynian structures) (López-Gómez and Arche, 1993a; Arche and López-Gómez, 1996), and a third phase during Middle Triassic represented by a long period of thermal subsidence (Sopeña et al., 1988; López-Gómez and Arche, 1993a; Arche and López-Gómez, 1996). These three stages were clearly differentiated in other basins of the Iberian Plate as well as in other parts of the western Tethys

(Fig. 3), although in this paper it will be shown that the beginning and ending of each phase differ between basins.

After the three syn-rift and post-rift extensional phases in the Iberian domain a period of post-rift thermal subsidence took place during the Early–Middle Jurassic with alkaline magmatism in the SE part of the Iberian Basin. Active rifting resumed during the late Oxfordian and persisted until the late Albian. This major rifting cycle can be subdivided into three minor syn-rift and post-rift pulses. From late Albian to late Maastrichtian time the Iberian Basin subsided during a thermal post-rift phase (Roca et al., 2001; Vergés ans Garcia-Senz, 2001; Salas and Casas, 1993).

3. The sedimentary record of the Iberian and Ebro Basins

This section describes the main lithological and sedimentological characteristics of the Permian and Triassic sediments in the Iberian and Ebro basins (Fig. 4, Tables 1, 2 and 3). Field sections are usually composite sections. A more detailed description can be found in Sacher (1966); Pérez-Arlucea and Sopeña (1985); Sopeña et al. (1988, 1995); Ramos (1979); Arche and López-Gómez (1989,1996, 1999b); López-Gómez (1985); López-Gómez and Arche, (1986, 1992a,b, 1993b, 1995, 1997); Muñoz et al. (1995); Van Wees et al. (1998); Rey et al. (1988); López-Gómez et al. (1998, 2002) among others for the Iberian Basin, and Jurado (1989, 1990); Arribas (1985); Arribas et al. (1985); De la Peña et al. (1977); Meléndez et al. (1995a); Ortí (1987, 1990) among others for the Ebro Basin.

The Iberian Ranges present very good outcrops from the lower Paleozoic basement to Quaternary rocks. To obtain the subsidence curves and stretching factors and phases we mainly used a detailed stratigraphic data base obtained from field studies of the Permian and Triassic listed in the previous paragraph, the Jurassic (Goy et al., 1976; Gómez, 1978; Gómez and Goy, 1979; Salas, 1989; Meléndez et al., 1990; Aurell et al., 1999) and the Cretaceous rocks (Mas, 1981; Canerot, 1982; Vilas et al., 1982; Meléndez, 1983). The Ebro Basin, however, shows an almost total lack of pre-Cenozoic outcrops. Instead, we used information from core and electrical well logs (Fig. 2B) obtained from different databases (IGME, 1987; Jurado, 1989), and correlated them with the surface data of the NE Iberian Ranges provided by Arribas (1985, 1987). The Anisian–Norian sediments of the Catalan Coastal Ranges and the Ebro Basin were correlated by López-Gómez et al. (1998), but the oldest

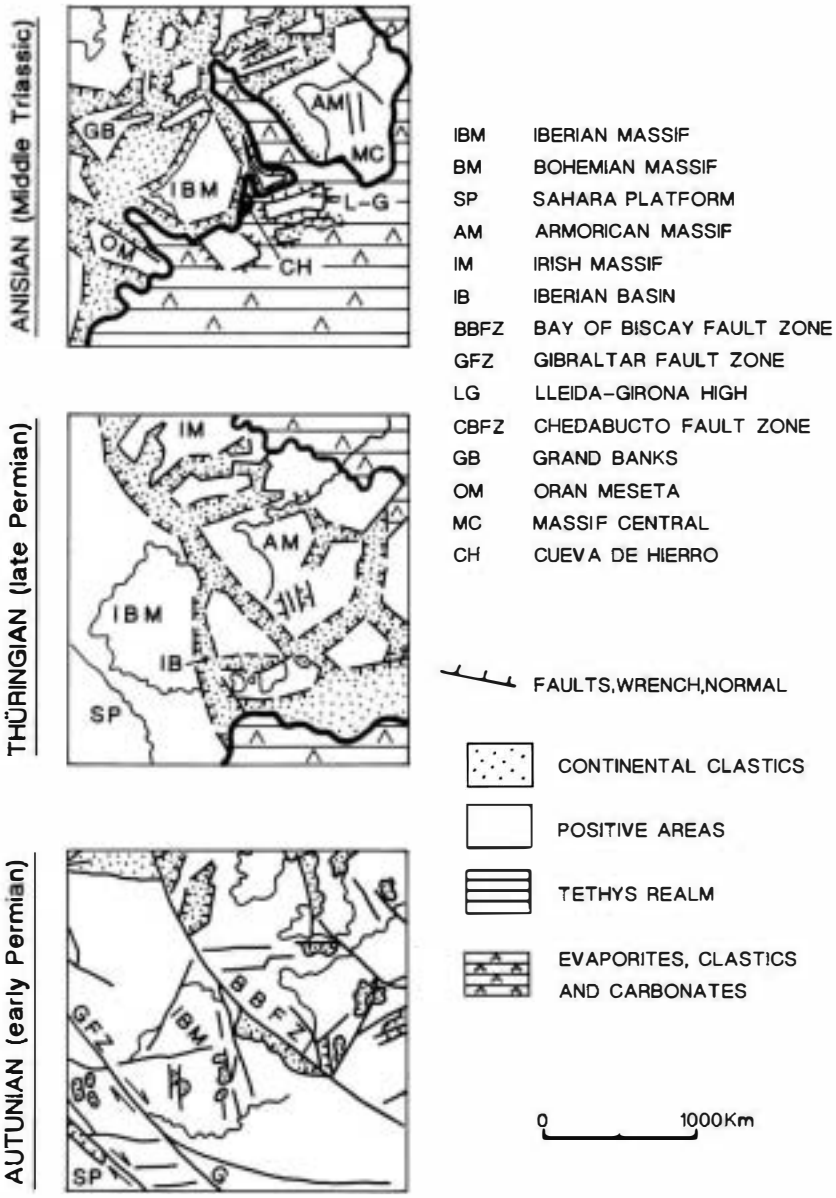

Fig. 3. Simplified paleotectonic-paleogeographic maps of the Western Tethys domain for the Autunian (Early Permian), Thüringian (Late Permian), Anisian (Middle Triassic). Modified from Ziegler (1988).

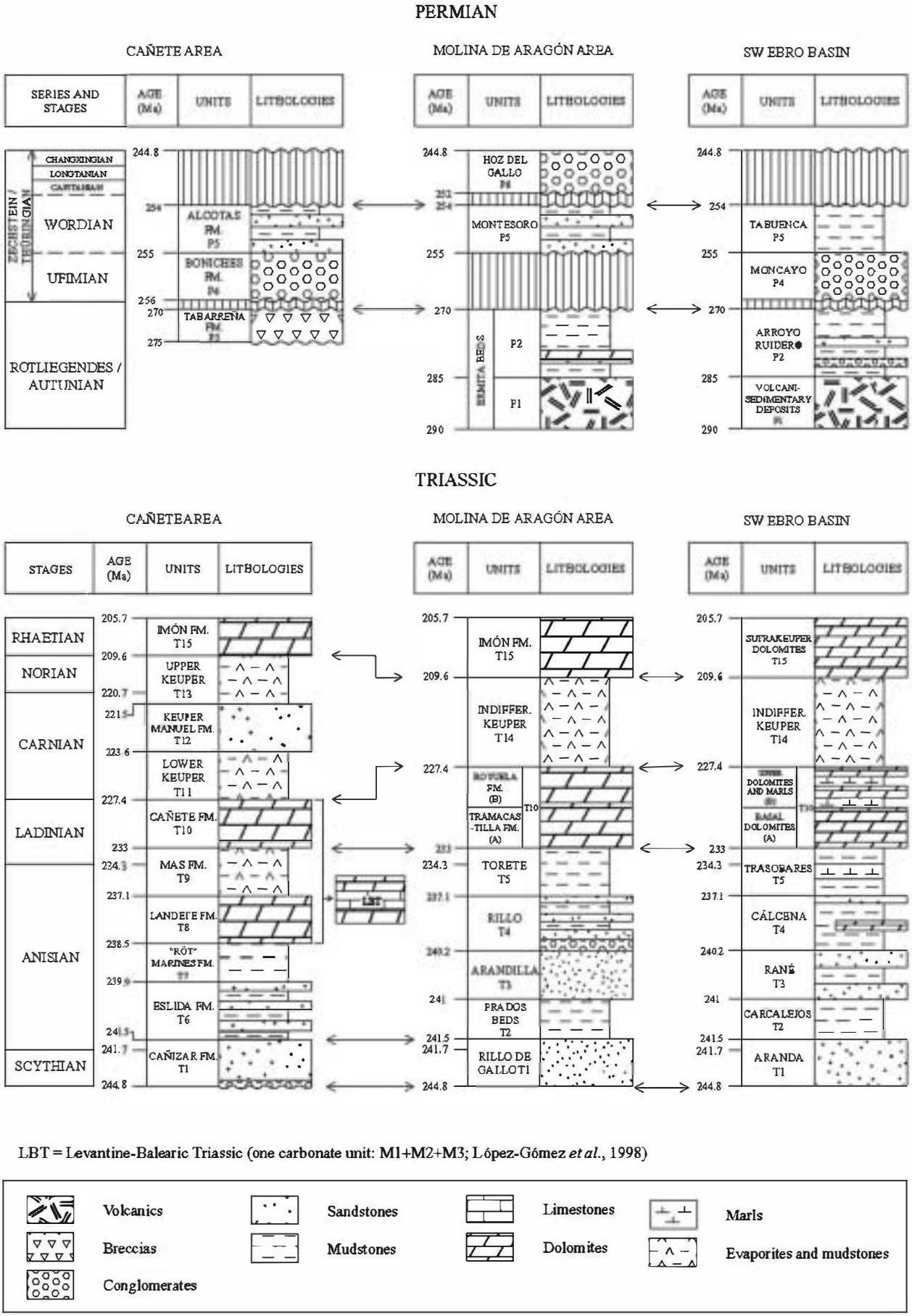

Fig. 4. Adopted stratigraphic subdivision for the Permian and Triassic sediments of the Ebro and Iberian basins. See also descriptions of the units in Tables 1, 2 and 3.

Table 1
Sketch of the main stratigraphical characteristics of the Permian sediments of the Iberian Ranges.

Description / Units		Age	Lithologic composition	Maximum thickness	Author (year)
Hoz del gallo conglomerates P6		Thüringian (Upper Permian)	Quartzite conglomerates and sandstone levels at the top	158 m	Ramos (1979)
Alcotas mudstones and sandstones fm. P5		Thüringian (Upper Permian)	Interbedded mudstones and sandstones and/or conglomerates	168 m	López-Gómez and Arche (1986, 1992a)
Montesoro beds P5		Thüringian (Upper Permian)	Breccias of several lithologies, siltstones alternating with sandstone and conglomerate beds and carbonate levels	94.5 m	Sacher (1966)
Boniches conglomerates fm. P4		Thüringian (Upper Permian)	Quartzite clasts with sandstone matrix	86 m	López-Gómez and Arche (1986, 1992a)
Tabarreña breccias fm. P3		Autunian (Lower Permian)	Quartzite pebbles and mudstone, sandstone matrix and slate fragments	21 m	López-Gómez and Arche (1986, 1992a)
Ermita beds	P2	Autunian (Lower Permian)	Alternance of siltstones and volcanic clasts and ferruginous carbonated levels. Siliceous dolomites with siltstones at the top	204 m	Sacher (1966)
	P1		Volcaniclastic sandstones, lava flows with volcanic conglomerates and some quartzite and slate pebbles	58 m	

See Fig. 4 for their stratigraphical location.

part of the Permian–Triassic, basically continental, sedimentary record of both areas has not been correlated in detail up to now, in spite of obvious similarities.

Most Permian and Triassic sediments can be broadly correlated throughout each basin. Concrete zones, however, have been taken as representative for both the Iberian and Ebro basins, where stratigraphy is synthesized in lithostratigraphical units correlated to absolute ages derived from the Gradstein et al. (1995) time scale.

3.1. Iberian Basin

Two zones in the NW and SE Iberian Basin have been chosen as the most representative of the Permian and Triassic stratigraphic record. The stratigraphic framework adopted in this paper is shown in Fig. 4 for the Cañete and Molina de Aragón zones.

Permian and Triassic sedimentation in the Iberian Basin records the beginning of extensional phases of the Alpine cycle. These sediments are dated by some fossil groups (ammonoids, conodonta, foraminifera, brachiopods e.g. López-Gómez et al., 1998, and pollen associations e.g. Doubinger et al., 1990; Sopeña et al., 1995; López-Gómez et al., 1998) that allow correlations throughout the basin and beyond including surface and well log data.

Permian sediments (P1–P6) are divided into three sequences separated by unconformities (Fig. 4). The lowest sequence (P1–P3) is not easy to correlate throughout the basin due to scarcity of fossils, especially in the upper part (P3), only lithological criteria and pollen

Table 2
Sketch of the main stratigraphical characteristics of the Triassic sediments of the Iberian Ranges.

Description / Units	Age	Lithologic composition	Maximum thickness	Author (year)
Imón dolomites fm. T15	Norian–Raethian (Upper Triassic)	Laminated dolomites with oolites, algal mats and evaporite beds	18 m	Goy et al., (1976)
Undifferentiated facies Keuper T14	Carnian–Norian (Upper Triassic)	Marls, gypsum and siltstones	324 m	This work*
Upper Keuper facies T13	Upper Carnian–Norian (Upper Triassic)	Clays and gypsum with some dolomitic bed	150 m	Ortí (1974)
Manuel sandstones fm. (Middle Keuper) T12	Carnian (Upper Triassic)	Sandstones and some mudstones	200 m	Ortí (1974)
Lower Keuper facies T11	Carnian (Upper Triassic)	Alternance of clays and gypsum with some marls	200 m	Ortí (1974)
Royuela dolomites, marls and limestones fm. T10B	Ladinian (Middle Triassic)	Dolomites with some limestone levels and marls at the top	45 m	Pérez-Arlucea and Sopeña (1985)
Tramacastilla dolomites fm. T10A	Ladinian (Middle Triassic)	Massive gray-ochre dolomites	45 m	Pérez-Arlucea and Sopeña (1985)
Levantine-balear triassic tlb	Anisian–Ladinian (Middle Triassic)	Gray dolomites with some limestone levels and marls in the middle part	140 m	López-Gómez et al. (1998)
Cañete dolomites and limestones fm. T10	Ladinian (Middle Triassic)	Dolomites and some limestones and marls	84 m	López-Gómez and Arche (1986, 1992a)
Mas clays, marls and gypsum fm. T9	Anisian–Ladinian (Middle Triassic)	From W to E clays and sandstones passing into marls, gypsum and dolomites	49 m	López-Gómez and Arche (1992a)
Landete dolomites fm. T8	Anisian (Middle Triassic)	Dolomites with some marls and evaporites beds	168 m	López-Gómez and Arche (1986, 1992a)
Marines clays, mudstones and marls fm. T7	Anisian (Middle Triassic)	Mudstones with marls, sandstone, limestone and gypsum beds	45 m	López-Gómez and Arche (1992a)
Eslida mudstones and sandstones fm. T6	Anisian (Middle Triassic)	Mudstones with some sandstones beds	663 m	López-Gómez and Arche (1992a)
Torete variegated mudstones and sandstones T5	Anisian–Ladinian (Middle Triassic)	Alternating siltstones and sandstones with many salt crystals pseudomorphs	41 m	Ramos (1979)
Rillo mudstones and sandstones T4	Anisian (Middle Triassic)	Alternance of sandstones and siltstones	197 m	Ramos (1979)
Río Arandilla sandstones T3	Anisian (Middle Triassic)	Sandstones with sandy siltstone beds	178 m	Ramos (1979)
Prados beds T2	Anisian (Middle Triassic)	Alternating sandstones and siltstones	45.3 m	Ramos (1979)
Rillo de Gallo sandstones T1	Scythian–Anisian (Lower–Middle Triassic)	Sandstones with some quartzite clasts and sandy siltstones	152 m	Ramos (1979)
Cañizar sandstones FM. T1	Scythian–Anisian (Lower–Middle Triassic)	Sandstones with some mudstone intercalations at the top and a conglomeratic level at the base	168 m	López-Gómez and Arche (1986, 1992a)

See Fig. 4 for their stratigraphical location.
* Defined in this work when there is not lithologic criteria of separation into T11, T12 and T13. Approximated thickness by partial dissolution.

Table 3
Sketch of the main stratigraphical characteristics of the Permian and Triassic sediments of the Ebro Basin.

	Description / Units	Age	Lithologic composition	Maximum thickness	Author (year)
Triassic	Suprakeuper dolomites = Imón FM T15	Norian–Raethian (Upper Triassic)	Laminated dolomites with oolites, algal mats and evaporite beds	110 m	Jurado (1989)
	Indifferentiated Keuper facies T14	Carnian–Norian (Upper Triassic)	Marls, gypsum and siltstones	248 m	This work*
	K3 = Upper Keuper T13	Upper Carnian–Norian (Upper Triassic)	Clays and gypsum with some dolomitic beds	55 m	Jurado (1989)
	K2 = Middle Keuper T12	Carnian (Upper Triassic)	Mudstones	130 m	Jurado (1989)
	K1 = Lower Keuper T11	Carnian (Upper Triassic)	Alternance of clays and gypsum with some carbonates	296 m	Jurado (1989)
	Upper dolomites and marls (B) T10	Ladinian (Middle Triassic)	Alternance of gray dolomites, marly dolomites and dolomitic marls	40 m	Arribas (1985)
	Basal dolomites (A)	Ladinian (Middle Triassic)	Grey dolomites	45 m	Arribas (1985)
	Upper Muschelkalk = Cañete FM T10	Ladinian (Middle Triassic)	Dolomites and some limestones and marls	126 m	Jurado (1989)
	Middle Muschelkalk = MAS FM T9	Anisian–Ladinian (Middle Triassic)	From W to E clays and sandstones passing into marls, gypsum and dolomites	315 m	Jurado (1989)
	Lower Muschelkalk = Landete FM T8	Anisian (Middle Triassic)	Dolomites with some marls and evaporitic beds	105 m	Jurado (1989)
	Trasobares mudstones and marls T5	Anisian–Ladinian (Middle Triassic)	Sandstones, mudstones, marls, dolomites and some gypsum embbeded into clay beds	40 m	Arribas (1985)
	Cálcena mudstones and sandstones T4	Anisian (Middle Triassic)	Mudstones with little sandstone beds and a dolomitic bed	80 m	Arribas (1985)
	Ranê sandstones and mudstones T3	Anisian (Middle Triassic)	Alternance of sandstone and mudstone beds	106 m	Arribas (1985)
	Carcalejos mudstones T2	Anisian (Middle Triassic)	Mudstones with some little sandstone beds	10 m	Arribas (1985)
	Aranda sandstones T1	Scythian–Anisian (Lower–Middle Triassic)	Sandstone beds with some conglomeratic beds at the base	150 m	Arribas (1985)
Permian	Tabuenca mudstones P5	Thüringian (Upper Permian)	Mudstones with some sandstone beds	108 m	Arribas (1985)
	Moncayo conglomerates P4	Thüringian (Upper Permian)	Conglomerates of quartzite clasts	15 m	Arribas (1985)
	Arroyo ruidero mudstones, sandstones and conglomerates P2	Autunian (Lower Permian)	Mudstones with some sandstone and conglomeratic beds, and piroclastic rocks	135 m	Rey and Ramos (1991)
	Volcani-sedimentary deposits P1	Autunian (Lower Permian)	Lava flows and volcaniclastics	90 m	De La Peña et al. (1977)

See Fig. 4 for their stratigraphical location.
* Defined in this work when there is not lithologic criteria of separation into T11, T12 and T13. Approximated thickness by partial dissolution of the evaporites.

data can be used for this correlation. These sediments, broadly denominated "Autunian facies" (see discussion in Arche et al., 2007), represent lacustrine, volcaniclastic, slope scree and alluvial fans deposited in small, isolated basins with very different infilling history (Ramos, 1979; Sopeñaet al., 1988; López-Gómez and Arche, 1994) (Table 1). The middle sequence (P4, P5) or "Saxonian" facies (Sopeña et al., 1988; López-Gómez et al., 2002) consists of a lower unit of conglomerates restricted to the centre of the basin of alluvial fan and braided river origin (Cañete zone) (López-Gómez and Arche, 1997), and an upper part containing intercalated sandstones and red mudstones deposited in meander and distal braided rivers and isolated ponds (Pérez-Arlucea and Sopeña, 1985; López-Gómez and Arche, 1993a,b; Arche and López-Gómez, 1999a). The term Saxonian should be discarded nowadays. The uppermost sequence (P6) constitutes the base of the "Buntsandstein facies" and consists of conglomerates of alluvial fan and braided fluvial origin (Ramos, 1979) succeeded by red sandstones of braided fluvial origin of Triassic age (Fig. 4 and Table 1).

In the Iberian Basin, the Permian–Triassic boundary is not well defined up to now. There is an almost continuous record of sediments probably without marked unconformities, as observed in most of Western Europe (López-Gómez et al., 2002). The Permian–Triassic boundary is somewhere between the basal conglomerates (P3) and the lower third of the sandstone formation (T1).

Triassic sediments in the Iberian Basin correlate well with the classical "Germanic Triassic megasequence" of Central Europe constituted by the Buntsandstein, Muschelkalk and Keuper Facies. Although there is no precise time equivalence between these sediments, the main sedimentary megasequences are equivalent in Western, Southern and Central Europe because most of the Pangean continent shows the extensional tectonic regime at the beginning of the Alpine cycle with two clear subsidence stages, one tectonic and other thermally induced (e.g. Stapel et al., 1996), corresponding to the Buntsandstein and Muschelkalk–Keuper facies respectively. Lithologies are very similar but their age boundaries are not.

During the Triassic four sedimentary sequences have been identified in the Iberian Basin bounded by hiatuses. The lowermost sequence (T1, T6) consists of two intervals: sandstones (T1) interpreted as sandy braided river deposits (Pérez-Arlucea and Sopeña, 1985; López-Gómez and Arche, 1986) and interbedded sandstones and red mudstones (T6) interpreted as distal braided meandering and ephemeral river deposits (Arche and López-Gómez, 1999b) (Table 2). The overlying sequence (T7, T8) consists of "Röt" facies (upper part of Buntsandstein facies) (T7) constituted by mudstones and marls of estuarine origin (López-Gómez and Arche, 1992b) and dolomites of the "lower Muschelkalk" (T8) interpreted as intertidal and shallow shelf deposits (López-Gómez et al., 1993, 1998). In the NW Iberian Ranges the interval T6–T7–T8 changes laterally into a siliciclastic, mostly continental sequence (Fig. 4) that consists, from base to top, of: (T2) that represent low energy fluvial deposits, (T3) that consists of sandy braided river deposits, and (T4) representing meandering river deposits (see Table 2). The third sequence (T9, T10) corresponds to the "middle-upper part of the Muschelkalk", represented respectively by mudstones, marls and gypsum (T9) of distal alluvial–sabkha origin (López-Gómez et al., 1993,1998) and dolomites (T10) of intertidal and shallow shelf deposits (López-Gómez et al., 1993, 1998) (T10). This sequence passes laterally into (T5) and (T10) in the NW Iberian Ranges (see Table 2), and reflects of a progresive transition from estuarine-mudflat deposits (T5) to intertidal and supratidal areas (T10). The uppermost sequence of the Triassic is represented by the Keuper facies (T11–T14) and the Imón Fm (T15). The Keuper (Ortí, 1974) consists of clays and evaporites of shallow marine origin (T11), sandstones of fluvial – to – coastal origin (T12) and evaporites of shallow marine origin (T13). The top of the Triassic

sequence (T15) consists of dolomites of intertidal and shallow shelf origin (Goy et al., 1976; Goy and Yébenes, 1977). T14 represents the Keuper facies when it is not possible to separate the formations defined by Ortí (1974) cannot be recognized.

3.2. Ebro Basin

The Permian–Triassic Ebro Basin is a wide, complex extensional structure that can be subdivided in three domains with different paleogeographic evolution (Fig. 2A). The western domain, west of Zaragoza, contains a thin but complete Permian–Triassic succession; the central domain, between Zaragoza and Lérida approximately, where subsidence was more important than the other two and a thick and complete Permian–Triassic succession is preserved and the eastern one, linking with the Catalan Basin south of the Lérida Paleozoic high, where the Permian–Triassic sediments are thin and were totally or partially eroded during the Alpine compressional tectonic phases.

Most of the Permian–Triassic sediments lie now under the Cenozoic cover of the Ebro Basin and can be studied only in commercial oil well logs and seismic profiles. They only crop out along the Aragonese branch of the Iberian Ranges (Arribas, 1985, 1987) as the SW marginal deposits of the basin, but a correlation can be drawn between this area, the Iberian Ranges, the Ebro Basin and the Catalan Ranges (Arche et al., 2004). The main biostratigraphic data published on these sediments can be found in De la Peña et al. (1977) and Díez et al. (1996) for the Permian (Doubinger et al., 1990) and in Gómez and Goy (1979), Torres (1990), Rey and Ramos (1991), Sopeña et al. (1995) and Meléndez et al. (1995b) for the Triassic.

The sediments of Early Permian age are found along the Aragonese branch of the Iberian Ranges and in the Caspe area in the subsurface of the Cenozoic basin (Arche et al., 2007). As there are almost no biostratigraphic data from the oil wells in the present-day Ebro Basin (Fig. 2B) the thick sequence at the base of some of them has not been taken into account in this study, although it can be Early Permian age. The undifferentiated Late Permian–Early Triassic continental sediments in the wells show two depocenters (N. Lérida and Caspe areas) (Fig. 2B) related with the Catalan Basin, and a central depocenter near Monzón area of much thinner sediments to the west of these depocenters. The outcrops along the Aragonese branch of the Iberian Ranges clearly show the pinch out of the sediments against the Ateca–Montalbán paleozoic high (Fig. 2A) and isopach maps are available in Arribas (1985) and Jurado (1989).

Marine sediments comprise most of the Muschelkalk and Keuper sediments and constitute a total of four evaporite-siliciclastic units

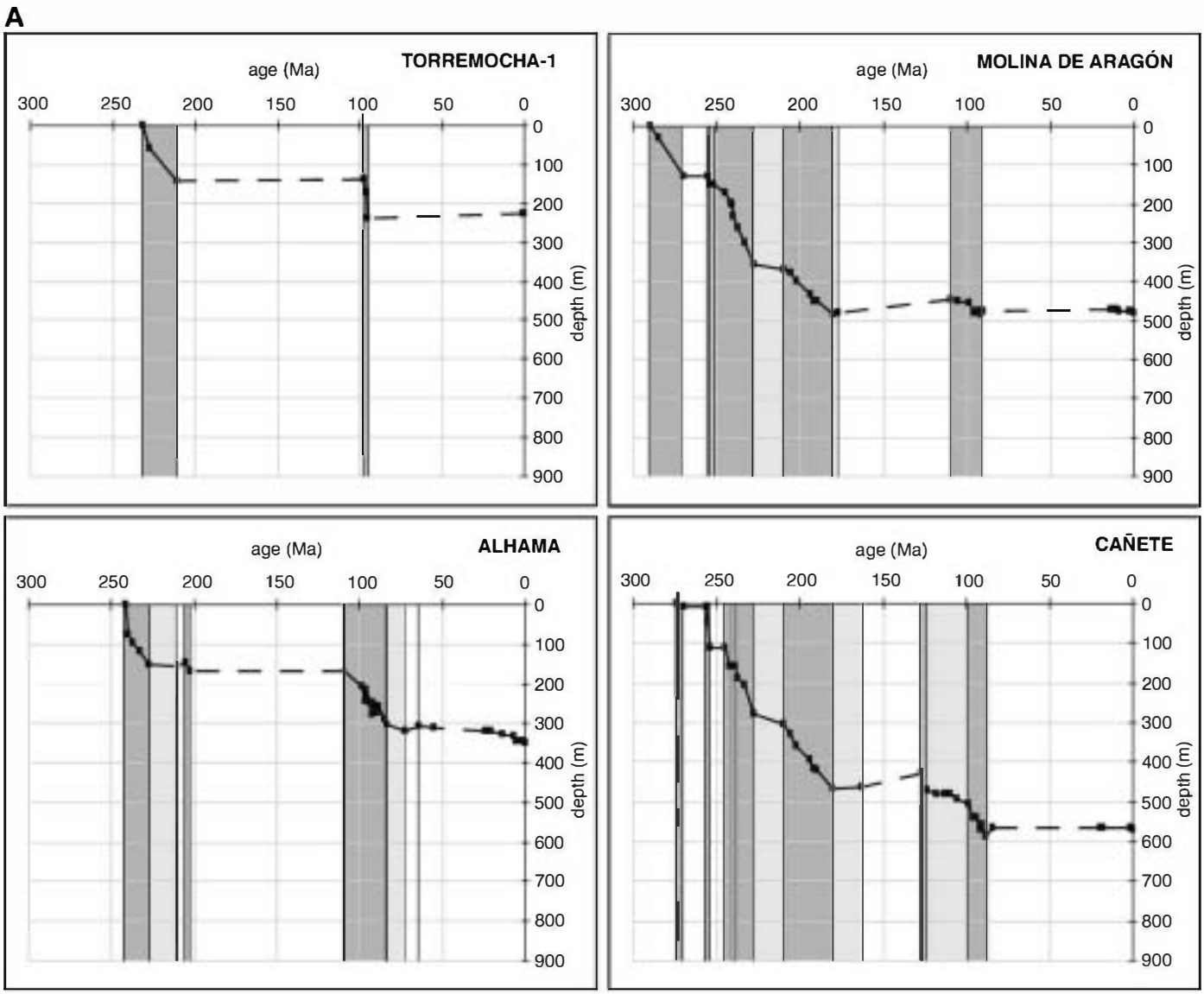

Fig. 5. A) Tectonic subsidence curves for the studied sections of the Iberian Ranges. See Fig. 2B for geographical locations. B) Continuation of A.

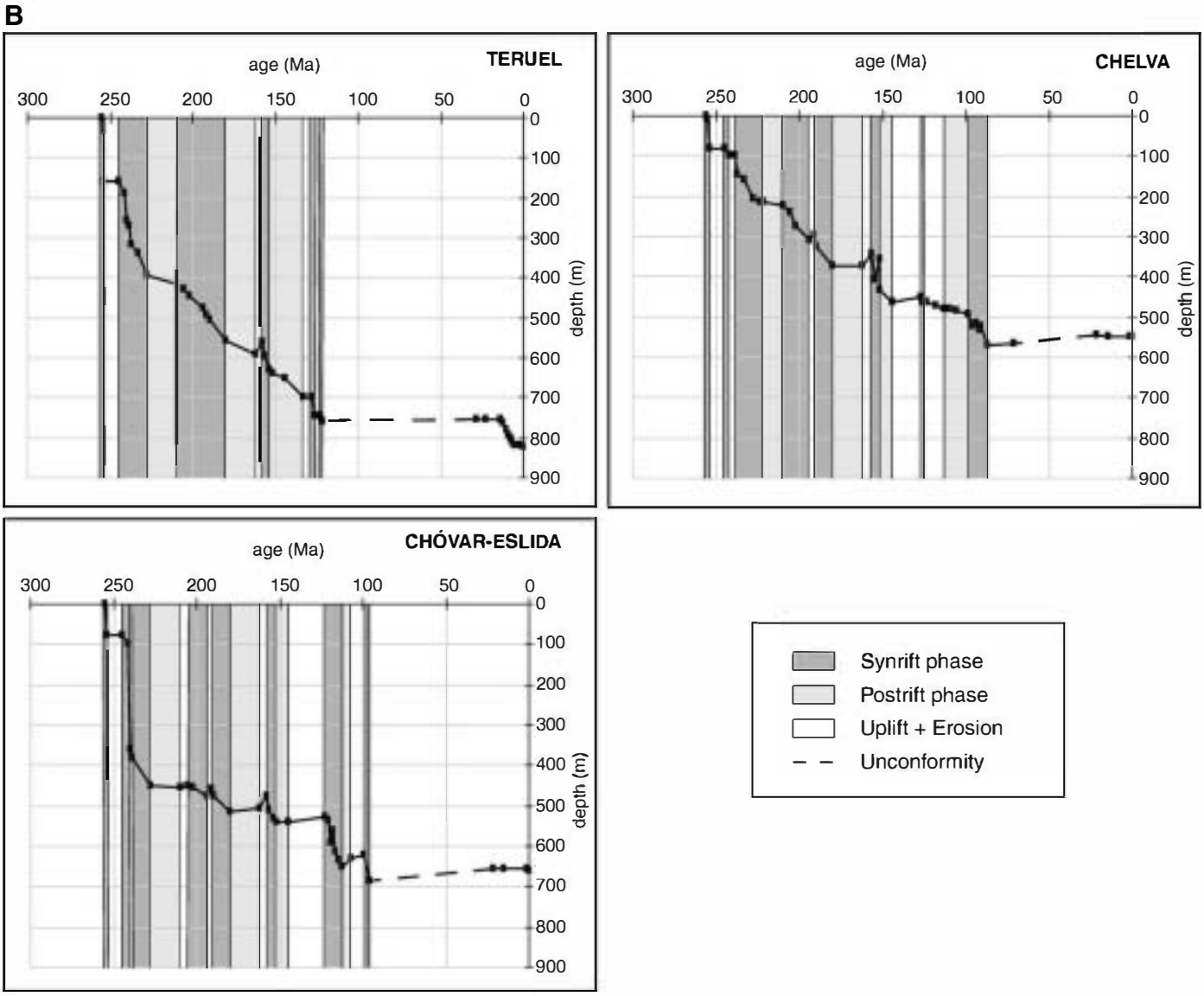

Fig. 5 (*continued*).

alternating with three carbonate ones. The evaporite-siliciclastic units are: the upper Buntsandstein or Röt facies (Anisian, Early Triassic), middle Muschelkalk (Anisian–Ladinian, Middle Triassic), lower Keuper (Carnian, Upper Triassic) and upper Keuper (Carnian–Norian, Upper Triassic). The carbonate units are: the lower Muschelkalk (Anisian, Middle Triassic), the upper Muschelkalk (Ladinian, Middle Triassic) and the Imón Formation (Rhaetian, Upper Triassic). These sediments show a sedimentary succession comparable to the one found in the Molina de Aragón area Central Iberian Basin domain (Fig. 4), in spite of the presence of the Ateca–Montalbán paleozoic high (Fig. 2A), to that separated the Ebro Basin from the Iberian Basin. A correlation is proposed by Arribas (1985) and was completed and slightly modified by Sopeña et al. (1988) (Fig. 4 and Tables 1, 2 and 3), in which the Saxonian facies, (Table 3) are time-equivalents of the (P4) and the (P5) in the Iberian Basin, the Buntsandstein facies are correlated with the (T1), (T2), (T3) and (T5) are the same levels in both basins. The Muschelkalk facies, that are represented only by its upper part, are correlated with (T10) of the Iberian Basin. Volcanic and volcanoclastic rocks are found in the Early Permian and the Late Triassic successions (Iago et al., 2001).

4. Subsidence analysis

To quantify the tectonic component of basement vertical movements of each studied basin for the Permian and Mesozoic, six sections and one well for the Iberian Ranges and seven wells for the Ebro Basin (Fig. 2B) have been analysed by means of backstripping technique (Steckler and Watts, 1978; Bond and Kominz, 1984). This technique is based on local isostasy, that corrects for the effect of sediment loading, and uses porosity-depth relationships (Sclater and Christie, 1980) to correct for compaction, obtaining the total subsidence, air-loaded tectonic subsidence and water-loaded tectonic subsidence curves.

The backstripping method is used to quantify the tectonic component of total subsidence in a basin and was defined by Steckler and Watts (1978). Eustatic sea-level variations amounted to a few tens of metres during the Mesozoic in this area, so its influence in subsidence quantification is very small and can be neglected; in any case, they have an effect which is equal for each well and surface section. Air-loaded subsidence is calculated from the stratigraphic record, adopting a local isostasy model to correct the effect for

Table 4
Permian and Triassic subsidence phases in the Iberian Ranges.

Age \ Sections		Torremocha-1	Molina de Aragón	Alhama	Cañete	Teruel	Chelva	Chóvar eslida
Triassic	Rhaetian	Uplift + erosion	Postrift phase (T14, T15)	Uplift + erosion	Synrift (T15–Jurassic)	Synrift (T15–Jurassic)	Synrift (T15–Jurassic)	Upli t + erosion
	Norian	Synrift 232-211 Ma. 144 m (T10, T14)		Postrift phase (T14)	Postrift (T14)	Postrift (T14)	Postrift (T11–T13)	Postrift (T14)
	Carnian							
	Ladinian		Synrift 244.8–227.4 Ma. 183 m (T1-T10)	Synrift 240.9–227.4 Ma. 150m1 (T3–T10)	Synrift 238.3–227.4 Ma. 119 m (T8-T10)	Synrift 244.8–227.4 Ma. 234 m (T1–T10)	Synrift 238.4–227.4 Ma. 105 m (T8–T10)	Synrift 238.5–227.4 Ma. 69 m (T8–T10)
	Anisian	----						Postrift (T7)
	Scythian	----		----	Synrift 244.8–241.8 Ma. 46m(T1)		Synrift 244.8–241.8 Ma. 17 m (T1)	Synrift 244.8–239.9 Ma. 287 m (T1,T6)
Permian	Thuringian	----	Synrift 255–254 Ma. 21 m (P5)	----	Synrift 256–254 Ma. 106m (P4, P5)	Synrift 255–254 Ma. 159 m(P5)	Synrift 256–254 Ma. 82 m (P4, P5)	Synrift 255–254 Ma. 75 m (P5)
	Autunian	----	Synri t 290–270 Ma. 129 m (P1, P2)	----	Synrift 274–270 Ma: 7 m (P3)	----	----	----

See Fig. 2B for geographical locations. Vertical striped indicate no sedimentation and/or erosion period.

sedimentary loading, stripping formation after formation from top to base of the section; corrections for compaction were made using standard porosity-depth relationships for each lithology.

Porosity-depth relations used for compaction correction were defined according to Sclater and Christie (1980) assuming a sandstone lithology for conglomerates, volcanic rocks and volcaniclastic sediments, a shale lithology for shales, a carbonate lithology for limestones and dolomites and finally, a halite-anhydrite lithology for the evaporites.

To isolate the effect of tectonics in the subsidence history, we had to correct for the effects of eustatic oscillations, paleobathymetry and sediment compaction with increasing loading. Paleobathymetry was estimated from sedimentary facies, fossils and depositional environments, always less than 75 m.

Since during the Cenozoic a different tectonic pattern than rifting (basin inversion in the Iberian Basin and foreland sedimentation in the Ebro Basin) and flexural and topographical effects took place (Van Wees et al., 1996; Van Wees and Beekman, 2000; Gaspar-Escribano et al., 2001); we omitted this period in our study. As Cenozoic inversion processes are not whitin the scope of this paper we will refer to the previous authors for a more detailed study of this process.

4.1. Iberian Ranges

Six stratigraphic sections (Alhama, Molina de Aragón, Cañete, Teruel, Chelva and Chóvar–Eslida) and one well (Torremocha-1) (Fig. 2B) were analysed in the Iberian Ranges.

In all sections tectonic subsidence curves (Fig. 5) show rapid subsidence phases followed by periods of slow subsidence (postrift) phases and some episodic uplifts associated to angular unconformities. Table 4 shows an scheme with results of the phases and tectonic subsidence values of these curves for the Permian and Triassic.

Only two sections present the first Autunian rapid tectonic subsidence phase: Molina de Aragón, from 290 to 270 Ma and approximately 130 m of tectonic subsidence, and Cañete from 274 to 270 Ma. During the Thüringian almost all sections show a second synrift phase from 256–254 Ma (Cañete and Chelva) and from 255–254 Ma (Molina de Aragón, Chóvar–Eslida and Teruel with the largest tectonic subsidence value: approximately 160 m). A third rifting phase takes place from Scytian to Ladinian in the Molina de Aragón and Teruel sections (244.8–227.4 Ma, including Buntsandstein and Muschelkalk facies). This phase has two pulses in Cañete and Chelva sections (244.8–241.8 Ma and 238.3–227.4 Ma), separated by an unconformity whereas in Alhama section it begins in the Anisian (240.9–227.4 Ma). A two-pulses phase is also interpreted for the Chóvar–Eslida section (244.8–239.9 Ma and 238.5–227.4 Ma) but a postrift phase is observed between both pulses.

Carnian and Norian times, corresponding with Keuper facies, appear as postrift phase in all sections, except for well Torremocha-1 that shows its first and only synrift phase from Ladinian to Norian (232–211 Ma, upper Muschelkalk and Keuper facies) with around 140 m and Molina de Aragón section that reaches the Rhaetian. The last rapid tectonic subsidence phase is shown in Cañete, Teruel and Chelva sections, appearing during the Rhaetian and lasting till Lower Jurassic, whereas in Torremocha 1 well and Alhama and Chóvar–Eslida sections this period corresponds with an uplift and subsequent erosion cycle.

4.2. Ebro Basin

Seven wells have been analysed in the Ebro Basin: Ejea-1, Monegrillo-1, Bujaraloz-1, Ebro-2, Caspe-1, Monzón-1 and Lérida-1 (Fig. 2B).

Backstripping analyses of these wells reveal a somewhat less complex subsidence history than in the Iberian Basin for the same studied period (Fig. 6). The data suggest one to three subsidence phases and a long lasting erosive period from Middle Triassic times to

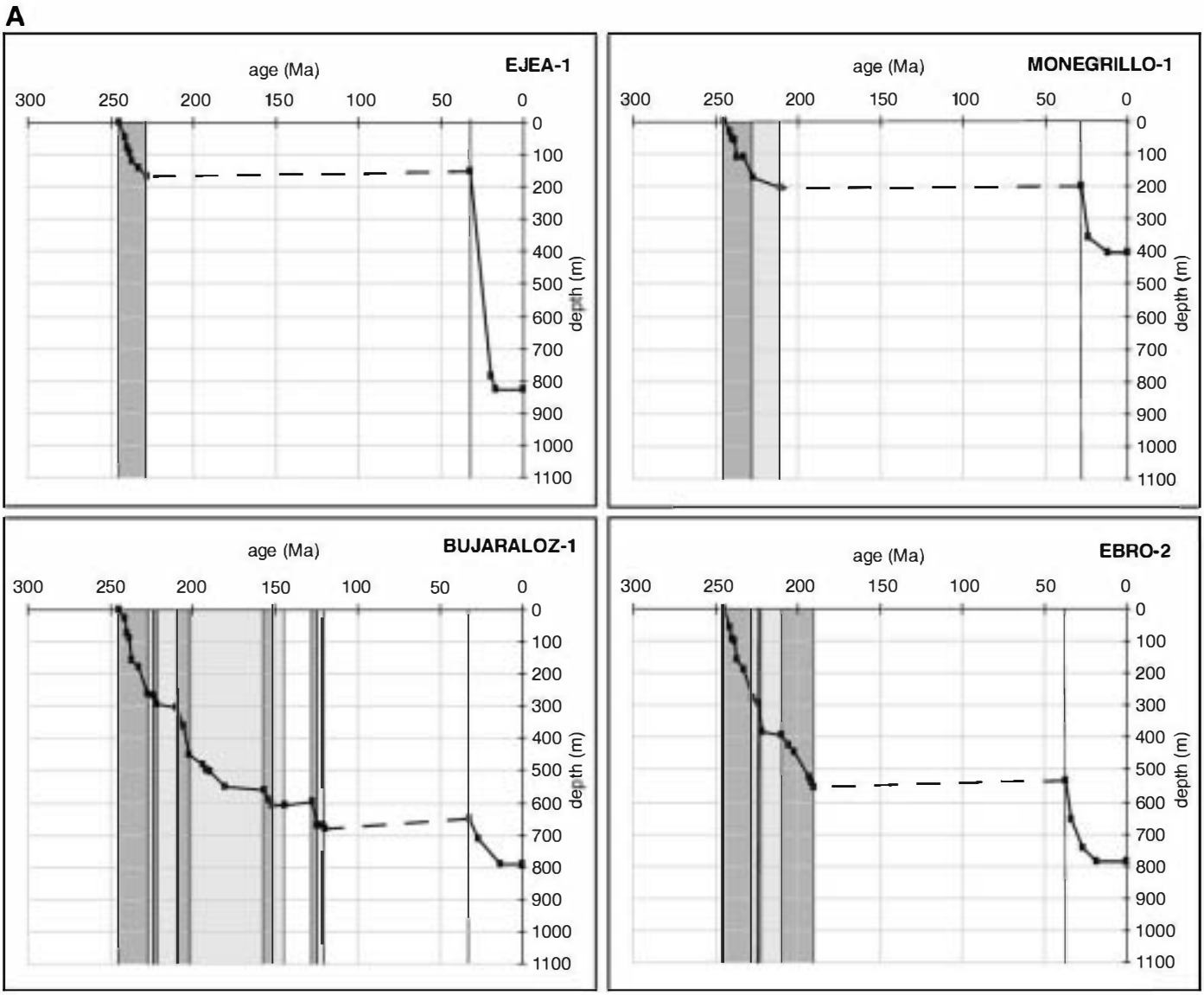

Fig. 6. A) Tectonic subsidence curves for the studied sections of the Ebro Basin. See Fig. 2B for geographical locations. B) Continuation of A.

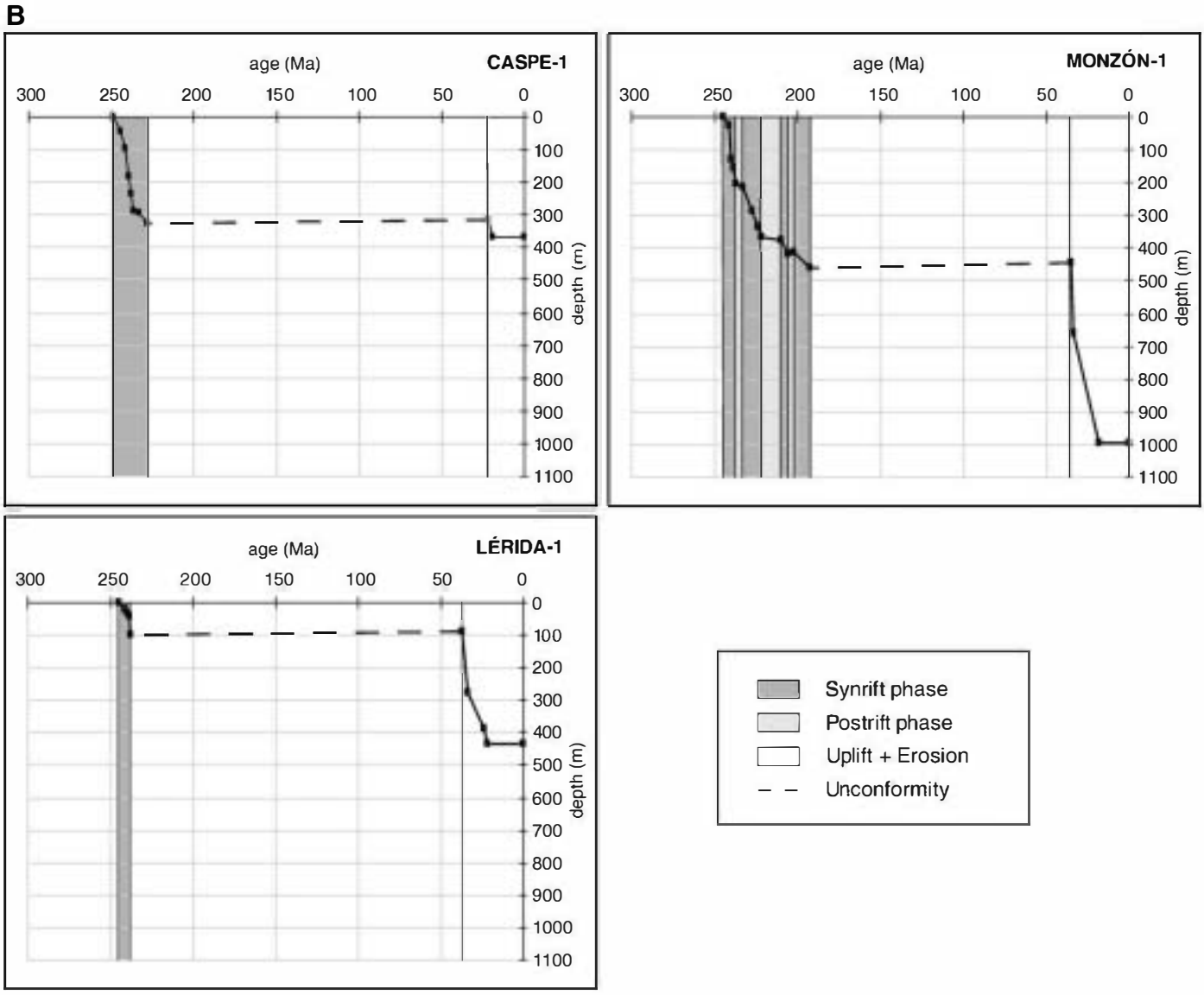

Fig. 6 (*continued*).

Eocene (Ejea-1, Caspe-1 and Lérida-1 wells). A summary of the subsidence analysis results are presented in Table 5. The presence of Early Permian sediments has been proved only in the Caspe-1 well (Arche et al., 2007) and has not been considered in this analysis.

During Early-Middle Triassic times an initial and rapid tectonic subsidence phase appeared in almost all wells, represented by the sediments of the Buntsandstein and Muschelkalk facies s. s. (244.8–227.4 Ma), with the exception of Caspe-1 well where Permian conglomerates at the base of the succession are included in the synrift phase (249–228 Ma); this phase reach up to approximately 320 m of tectonic subsidence. This phase is interrupted in the Lérida-1 well due to later erosion (Early Triassic to Middle Triassic) and include the Buntsandstein and lower Muschelkalk facies sediments reaching about 100 m of tectonic subsidence. A later postrift phase was preserved partially from Tertiary erosion in Monegrillo-1, Bujaraloz-1 and Ebro-2 wells and comprises most of the Keuper facies (Carnian to Norian) in Monegrillo-1 well, and the lower Keuper in Bujaraloz-1 and Ebro-2 wells.

A second synrift phase appears in Bujaraloz-1 and Ebro-2 wells that included middle Keuper facies sediments (Carnian) reaching around 30 m and 90 m of tectonic subsidence respectively, and a second postrift phase appears in Bujaraloz-1, Ebro-2 and Monzón-1 during the Norian (upper Keuper). In Monzón-1 well, the first synrift phase is shown by sediments from 244.8 to 237.1 Ma, including the Buntsandstein and lower Muschelkalk facies, while the middle Muschelkalk is represented by a postrift phase. The second synrift phase comprises the upper Muschelkalk and the lower part of the Keuper facies (233–221.5 Ma).

There is a third rapid tectonic subsidence phase during the Rhaetian in Monzón-1 well (209.6–205.7 Ma and about 40 m of tectonic subsidence), and reaching the Lower Jurassic in Bujaraloz-1 and Ebro-2 wells.

Ejea-1 and Caspe-1 wells show a longlasting erosion from 228 Ma (Ladinian, that corresponds to the upper Muschelkalk) onwards and Lérida-1 well from 237.8 Ma (upper Anisian, lower Muschelkalk) onwards, whereas Monegrillo-1 well shows this erosion from the Rhaetian.

5. Comparison of subsidence evolution of Iberian and Ebro Basins: synrift and postrift stages, and geometry

The results from the analysis of the synrift and postrift subsidence phases for Permian and Triassic times have been correlated between

Table 5
Permian and Triassic subsidence phases in the Ebro Basin.

Age	Section	Ejea-1	Monegrillo-1	Bujaraloz-1	Ebro-2	Caspe-1	Mónzon-1	Lérida-1
Triassic	Rhaetian	Uplift + erosion	Uplift + erosion	Synrift (T15-Jurassic)	Synrift (T15-Jurassic)	Uplift + erosion	Synrift 209.6-205.7 Ma. 38 m (T15)	Uplift + erosion
	Norian		Postrift phase (T14)	Postrift (T13)	Postritft (T13)		Postrift (T13)	
	Carnian			Synrift 223.6-221.5 Ma. 27 m (T12)	Synrift 223.6-221.5 Ma. 88 m(T12)		Synrift 2.533-221 Ma. 152 m (T10-T12)	
				Postrift (T11)	Postrift (T11)			
	Ladinian	Synrift 244.8-228 Ma. 170 m (T1-T10)	Synrift 244.8-227.4 Ma. 175 m (T1-T10)	Synrift 244.8-227.4 Ma. 263 m (T1-T10)	Synrift 244.8-22 7.4 Ma. 277 m (T1-T10)	Synrift 249-228 Ma.323 m (P6-T10)	Postrift (T9)	
	Anisian						Snyrift 2.144.8-237 M a. 204 m (T1-T8)	Synrift 244.8-237.8 Ma. 98 m (T1-T8)
	Scythian							
Permian	Thuringian	-- --	-- --	-- --	-- --	-- --	-- --	-- --
	Autunian	-- --	-- --	-- --	-- --	-- --	-- --	-- --

See Fig. 2B for geographical locations.

the Iberian and Ebro basins (Tables 4 and 5) and the synrift stages I–V have been identified in every section and well (Fig. 7).

(Stage I–II) In the beginning, during the Autunian times (stage I), minor subsidence is observed for the SW boundary of the Iberian Basin. For the Ebro Basin, two small semigrabens with Autunian sediments have been described in field sections by Monrose (1968), De la Peña et al. (1977), Del Olmo et al. (1983) around the Ateca area. As suggested by the distribution of tectonic subsidence for the NW side of the Iberian Basin (Fig. 7) and the geometry of the small, isolated half grabens of this age, it is probable that the small basins found in the outcrops along the SW part of the Ebro Basin, close to the main basin boundary faults, could be also present but not identified yet in subsurface in this area; this is in agreement with considerable volcanic activity along the Ateca–Montalban high.

As can be seen in the Molina de Aragón section, a major angular unconformity spanning at least 25 Ma separates stage I from stage II. This is probably due to a tilting and uplift of the Autunian basins, most likely after a late thermal event related to stage I extension, a mechanism proposed by Royden and Keen (1980) for a similar situation in the Triassic of the continental margin of eastern Canada. Stage II is marked by slightly larger tectonic subsidence but it is localised in small pockets, where subsidence varied from a few tens of meters to more than 300 m (Sopeña et al., 1988).

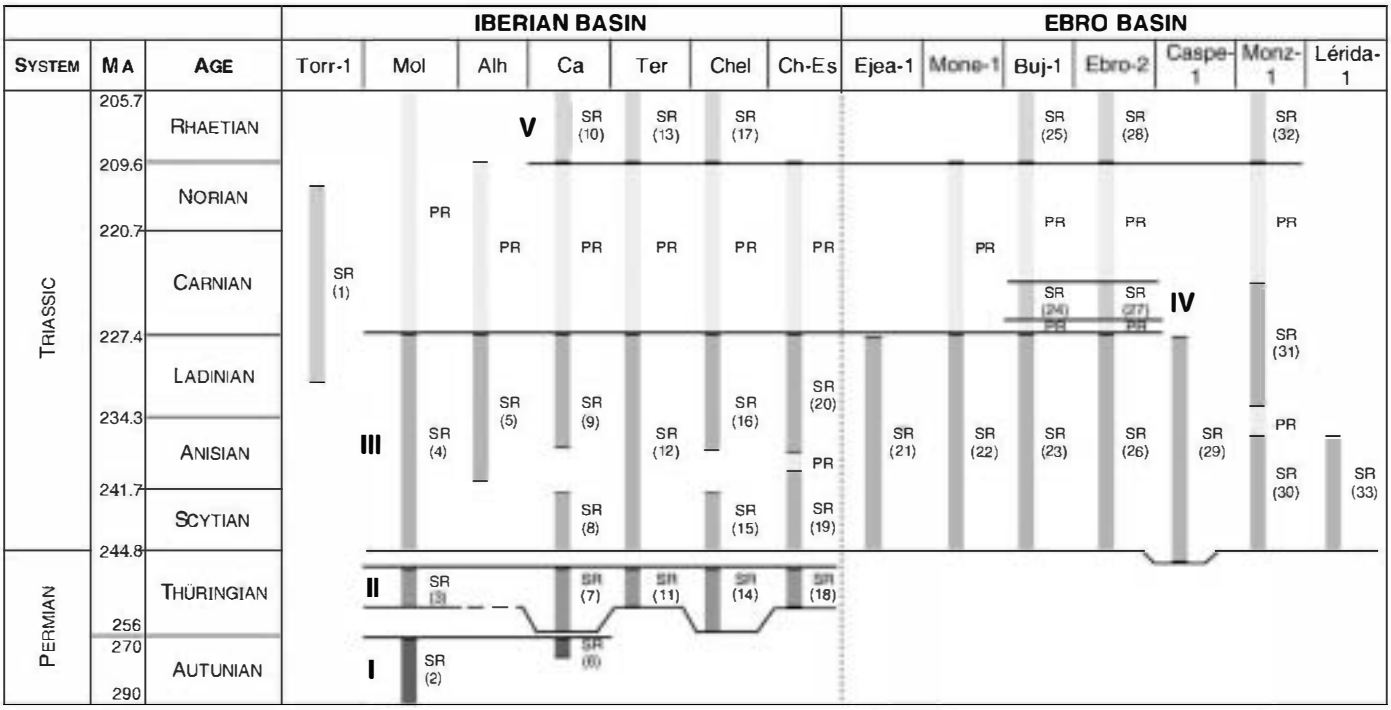

Fig. 7. Synrift and postrift subsidence phases in all the sections and wells studied in the Iberian and Ebro basins in the Permian–Triassic period. SR— synrift phase; PR— postrift phase. I to V indicate the main general differentiated phases for both studied basins. β,δ values respectively are: Iberian Basin (1) 0.941, 1.029; (2) 0.989, 1.03; (3) 1.026, 1.011; (4) 0.996, 1.042; (5) 0.87,1.022; (6) 1.001,1.002; (7) 1, 1.027; (8) 1, 1.101; (9) 1.001,1.026; (10) 0.88,1.017; (11) 0.997,1.04; (12) 0.992,1.056; (13) 1.062,1.032; (14) 1.002, 1.02; (15) 1.001,1.005; (16) 0.998,1.025, (17) 0.999,1.015; (18) 0.984,1.017 (19) 1.002,1.067 (20) 0.915, 1.009. Ebro Basin (21) 0.995,1.051; (22) 0.997,1.046; (23) 0.996,1.068; (24) 0.977, 0.998; (25) 1.106, 1.063; (26) 0.997, 1.074; (27) 0.999, 1.02; (28) 1.003,1.034; (29) 1.003, 1.1; (30) 1.001, 1.052; (31) 0.998, 1.037; (32) 0.996, 0.999; (33) 1.001, 1.018. See Fig. 2B for the geographical location of the sections and wells.

(Stage III) During this stage the Ebro Basin developed as a single, major extensional structure (basal Triassic to early Anisian). Permian conglomerate sediments found in the lower part of the Caspe-1 well indicate that synrift sediments of stage III started earlier in this area than in the rest of the Ebro Basin (Fig. 10). In the Ebro Basin, the presence of small isolated basins of Autunian age observed in the field, indicate that a basin boundary normal fault system developed along the NE border of the Ateca high, an uplift basement block separating the Iberian and Ebro basins.

(Stage IV–V) A lower Carnian synrift phase (IV) has only been observed in the central area of the Ebro Basin, and an isolated phase from 232 to 211 Ma appear in the SW boundary of the Iberian Basin, shown in Torremocha-1 well (Fig. 7). For most of the wells, the Carnian and Norian times represent a general postrift phase that is manifested in all the Iberian basin except for the SW border as will be discussed later. This stage shows an important change in the style of subsidence. For the first time, considerable postrift subsidence is observed, in particular in the Teruel section (Ter) in the Iberian Basin and Bujaraloz-1 in the Ebro Basin. The beginning of a generalized heatloss could justify this notable change. Very big carbonate platform or sabkha deposits that covered hundreds of kilometres (López-Gómez et al., 1998) were the surface response of a basin that at the end of the Triassic had unified both previously independent Iberian and Ebro basins (Fig. 7).

The observed Rhaetian synrift phase (V) was probably the most homogeneous one in both basins and is clearly visible in the surface sections.

From Fig. 7, a first obvious difference between both basins is that the two Permian synrift phases (I and II) of the Iberian Basin are not observed in the Ebro Basin, except in Caspe-1 well, where the phase II is represented and maybe phase I. These early synrift phases are generally shorter in time than the later phases during the Triassic.

Furthermore, a general characteristic of the Iberian Basin is the multiphase succession of synrift episodes since the opening of the basin (stage I–II) until the end of the Ladinian (stage III). This strongly contrasts with the general seemingly single phase (III) observed in the Ebro Basin for the same period of time (Fig. 7). The absence of one or both early rifting phases in different areas indicate the independent evolution of semigrabens during their development. The transition towards a single unified basin occurs only after stage III. Based on field mapping and relative magnitudes of tectonic subsidence from our analysis, a synthetic cross-section can be drawn (Fig. 8), which clearly illustrates the evolution of semigraben structures in stages I–III, and the uniform basin evolution after stage III. The evolution of independent semigraben structures is clearly supported by the markedly strong lateral variations in synrift subsidence, which can be most likely be attributed to the occurrence of one or two major crustal scale NE dipping master faults (Fig. 8), bounding the SW sides of the Iberian and Ebro basins.

Semigraben evolution can explain the major features of the origin and evolution of the Permian–Triassic Iberian and Ebro basins, as suggested earlier by Arche and López-Gómez (1996), which is also supported by the asymmetric shape of the contours of the isopach maps for the Permian and Early Triassic sediments (Arche and López-Gómez, 1999a). A hypothetical reconstrution with only one major crustal scale simple shear zone, flattening out at a depth probably not exceeding 15 km, is shown in Fig. 8. As can be seen in this figure, extension propagated from the SW to the NE with time for the stages I–III. A fixed point (FP) for the reconstrution is located in the southwestern footwall or "breakaway" (cf. Gibbs, 1984, 1987).

6. Forward modelling

After calculating the total subsidence and air-loaded tectonic subsidence curves by the backstripping method, we use a forward model (Van Wees et al., 1996, 1998) to calculate thinning factors (δ for

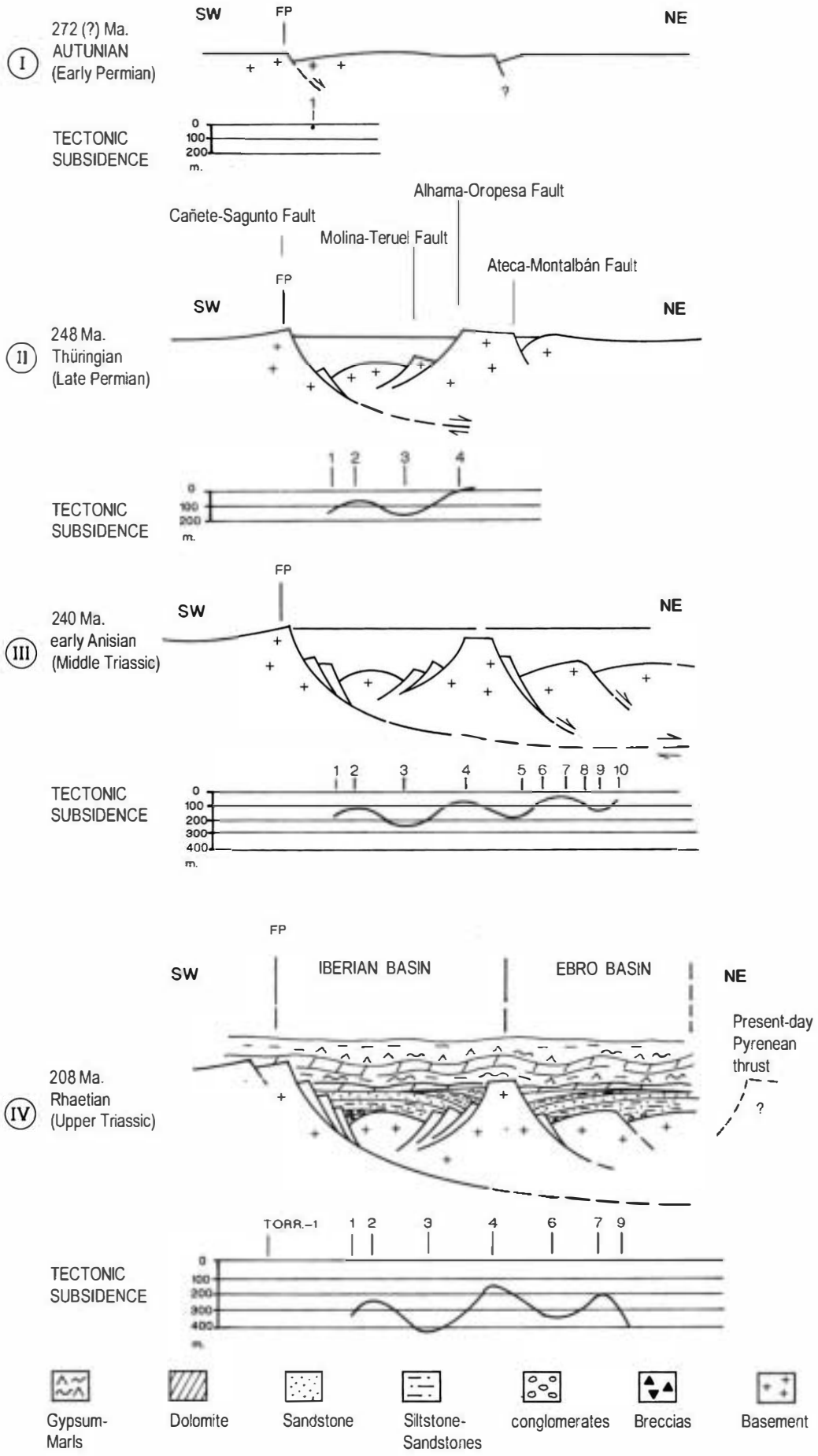
I
272 (?) Ma.
AUTUNIAN
(Early Permian)
SW
FP
NE
TECTONIC
SUBSIDENCE
0
100
200
m.
II
248 Ma.
Thüringian
(Late Permian)
Cañete-Sagunto Fault
Molina-Teruel Fault
Alhama-Oropesa Fault
Ateca-Montalbán Fault
SW
FP
NE
1 2 3 4
TECTONIC
SUBSIDENCE
0
100
200
m.
III
240 Ma.
early Anisian
(Middle Triassic)
FP
SW
NE
1 2 3 4 5 6 7 8 9 10
TECTONIC
SUBSIDENCE
0
100
200
300
400
m.
IV
208 Ma.
Rhaetian
(Upper Triassic)
FP
SW
IBERIAN BASIN
EBRO BASIN
NE
Present-day
Pyrenean
thrust
?
TORR.-1
1 2 3 4 6 7 9
TECTONIC
SUBSIDENCE
0
100
200
300
400
m.
Gypsum-
Marls
Dolomite
Sandstone
Siltstone-
Sandstones
conglomerates
Breccias
Basement

Table 6
Parameters used in the forward model (obtained from Van Wees and Stephenson, 1995).

Parameter	Value
Initial crustal thickness	32 km
Initial lithospheric thickness	110 km
Asthenospheric temperature	1333 °C
Thermal diffusivity	1×10^{-6} m^2 s^{-1}
Surface crustal density	2800 kg m^{-3}
Surface mantle density	3400 kg m^{-3}
Water density	1030 kg m^{-3}
Thermal expansion coefficient	3.2×10^{-5} °C

crust, β for subcrustal lithosphere) for each extensional phase and for each section or well.

To carry out the forward modelling we estimate an initial crustal thickness of 32 km corresponding to the present-day value beneath the Iberian Massif (Banda et al., 1983) and adopted for the Iberian Ranges by Salas and Casas (1993), Van Wees and Stephenson (1995) and Van Wees et al. (1998), and an initial lithospheric thickness of 110 km used in the Iberian Basin by Morgan and Fernández (1992), Van Wees and Stephenson (1995) and Van Wees et al. (1998). Other parameters used in the modelling and obtained from Van Wees and Stephenson (1995) are shown in Table 6.

The forward modelling technique (usually called inverse approach), is based on lithospheric stretching assumptions (McKenzie, 1978; Royden and Keen, 1980) using the factor δ for crustal stretching and β for subcrustal stretching. The model used in this paper allows an unlimited number of stretching phases and optimises the stretching parameters with respect to the subsidence data (Van Wees et al., 1998 for details). In a rifting phase either uniform lithospheric stretching (McKenzie, 1978: $\beta=\delta$) or two-layered stretching (Royden and Keen, 1980: $\beta\neq\delta$) can be used.

As mentioned previously, the Cenozoic deposits in the Ebro Basin and the margins of the Iberian Range were deposited under a compressional regime in foreland basins with flexural isostatic compensation in contrast to Permian and Triassic sediments deposited under an extensional tectonic regime. Therefore, our forward modelling method does not apply to data younger than 65 Ma.

6.1. Two-layer stretching (Figs. 8, 9)

Earlier quantitative subsidence studies in the Iberian Basin, have shown that often the postrift subsidence is conspicuously low or even absent with unconformities in what should be the postrift sequence. Uniform lithospheric stretching, therefore, is bound to be inconsistent with observed data. Van Wees et al. (1998, their Fig. 10) explained these unconformities by phases of thermal uplift, in a two-layer stretching process produced by subcrustal stretching during the postrift phase ($\beta>1$, $\delta=1$). In this paper we apply two-layered stretching only in the synrift stages, to see if differences between crustal and subcrustal stretching agree with a simple shear crustal shear zone resulting in differences between crustal and subcrustal stretching.

Fig. 9 shows an example of uniform (one-layer) and depth-dependent (two-layer) stretching results for two selected sections in the Iberian and Ebro basins. Generally, depth-dependent stretching yield a better fit to the observed data. As will be clear from the modelling results, this approach will give rise in many cases to subcrustal stretching values which are less than 1. This evidently seems a contradiction, which will be discussed later.

6.2. Iberian Ranges

As we mentioned earlier, the two-layer stretching model ($\beta\neq\delta$) used in the forward modelling fits better than the uniform stretching one ($\beta=\delta$). Successive short stretching pulses with values of β and δ not greater than 1.062 and 1.067 respectively have been quantified in the process of modelling (Fig. 10).

An initial Autunian rifting (290–270 Ma) developed in Molina de Aragón and Cañete sections, with a shorter time span in the second (274–270 Ma). β values slightly smaller than 1 or nearly 1 and δ values of 1.03 and 1.002 respectively are found.

Three later synrift phases developed simultaneously in almost all the studied sections.

The first phase, from 256 to 254 Ma in Cañete and Chelva sections and 255 to 254 Ma in Molina de Aragón, Teruel and Chovar–Eslida sections, shows β values from slightly smaller than 1 to 1.026 in Molina de Aragón section, and δ values ranging from 1.011 in Molina de Aragón section to 1.040 in Teruel section.

The second phase (244.8–227.4 Ma) is observed in Molina de Aragón and Teruel sections and shorter in time in Alhama, Cañete and Chelva sections. This phase, when complete, shows β values smaller than 1 and δ values from 1.042 to 1.056, but when it is shorter in time, as in Alhama section, β value corresponds also to the lowest (0.87) value observed in the Iberian Ranges. For the previously described two-pulses of this phase of the Chóvar-Eslida section β and δ values are 1.002 and 1.067 for the first pulse and 0.915 and 1.009 for the second pulse respectively in both cases. The 1.067 δ value of the first pulse is the largest observed for this phase in the selected sections of the Iberian Basin.

The third and last synrift phase (from 209.6 Ma to 180.1 Ma) is observed in Cañete, Teruel and Chelva sections. β values range from 0.88 in Cañete section to 1.062 in Teruel section and δ values range from 1.015 to 1.032 in Chelva and Teruel sections respectively.

Torremocha-1 well shows only one rapid subsidence phase from 232 to 211 Ma followed by an uplift and subsequent erosion. It shows a β value of 0.941 and δ value of 1.029.

6.3. Ebro Basin

The two-layered stretching model also fits better in this basin than uniform stretching model, however, differences between both models are not so marked than in the Iberian Basin, as shown in Fig. 9.

The analysis shows three synrift phases (Fig. 11):

The first synrift phase, from Lower to Middle Triassic (244.8–227.4 Ma) is observed in almost all wells. Bujaraloz-1 well shows the lowest value of β (0.996) and Ebro-2 well the greatest for δ (1.074). Ejea-1 and Caspe-1 wells show this phase from 244.8 to 228 Ma due to the subsequent erosion, with β values of 0.995 and 1.003 and δ values of 1.051 and 1.1 respectively, and Lérida-1 well shows the shortest one (244.8–237.1 Ma) due to a longer erosion.

The second synrift phase comprises the middle Keuper facies sediments of Carnian age (223.6–221.5 Ma). It appears in Bujaraloz-1 and Ebro-2 wells, that show β values of 0.977 and 0.999 and δ values of 0.998 and 1.02 respectively.

In the previously described two lower synrift phases of the Monzón-1 well, β and δ values are 1.001 and 1.052, and 0.998 and 1.037 respectively from the lower to the second phase.

The third rapid subsidence phase is recorded in Bujaraloz-1, Ebro-2 and Monzón-1 wells. It comprises the Rhaetian–Lower Jurassic interval, and the β values are smaller than 1 to 1.106, the largest

Fig. 8. Comparison between the Iberian and Ebro basins evolution in relationship with the tectonic subsidence values observed from the Autunian, Thüringian, early Anisian and Rhaetian phases. Numbers indicate sections or wells from where tectonic subsidence were obtained (see also Fig. 2B for the geographical locations, Fig. 7 for more detail of the differentiated phases and Fig. 12 for the stretching factor values). 1 — Cañete (Ca), 2 — Chelva (Che), 3 — Chovar–Eslida (Cho–Es), 4 — Teruel (Ter), 5 — Alhama (Alh), 6 — Caspe-1, 7 — Bujaraloz-1 (Buj-1), 8 — Monegrillo-1 (Moneg-1), 9 — Ebro-2, 10 — Monzón-1 (Monz-1). FP — "Fixed point".

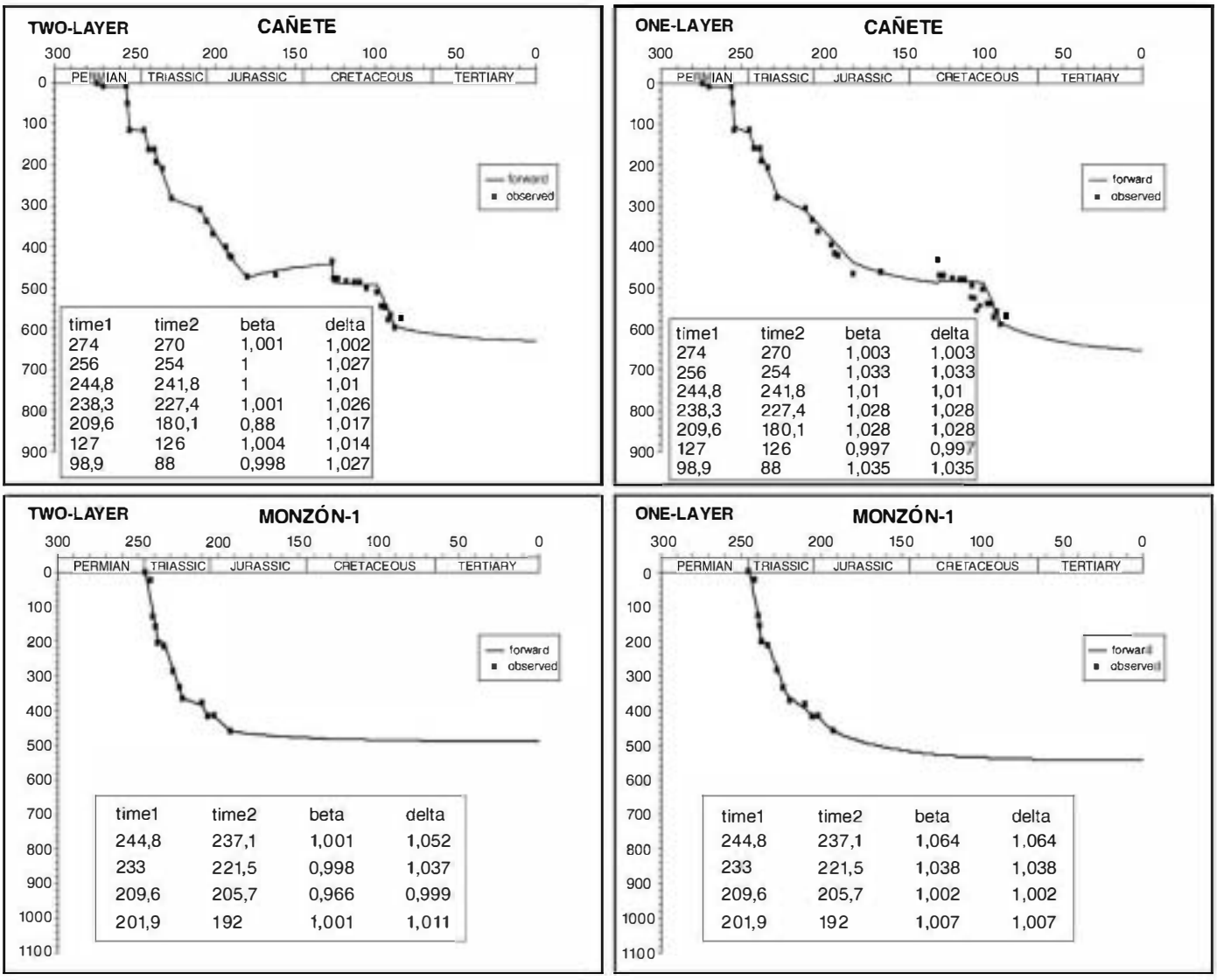

Fig. 9. Comparison between two-layer and one-layer stretching models in two selected sections in the Iberian and Ebro basins. It can be observed that two-layer modelling fits much better for the sections of the Iberian basin than one-layer modelling, whilst differences between both modelling are not so evident for the Ebro Basin selected wells.

value obtained for Bujaraloz-1 well, and the δ values are from 0.999 in Monzón-1 well till 1.063 in Bujaraloz-1 well.

The proposed two-layer model for the extensional process during the Permian–Triassic period in the Iberian Basin can be constrained more precisely by considerations of level of necking, paleotopography of the basins and degree of coupling of the two lithospheric layers.

The Iberian Rift basins had energetic reliefs in both shoulders, with a topographic difference of at least 600–700 m between the high footwall rift shoulders and the low-lying hanging-wall basins, as is clearly indicated by the differences in sediment thickness in both areas. For the Late Permian–Early Triassic period (256–230 Ma.), a cratonic configuration of the lithosphere can be assumed for this area (Van der Beek et al., 1994; Cloetingh et al., 1995; Ter Vooede et al., 1998; Chéry et al., 1992) because more than 40 Ma. have spanned since the last granitic intrusions took place in the studied area during the late Variscan events and the lithospheric thermal regime has returned to a "normal" configuration by heat loss in this long period of time.

A deep level of lithospheric necking is, therefore, most likely leading to strong upwards flexure of the rift shoulders by isostatic response contemporaneous to active extension (Cloetingh et al., 1995). This is in agreement with the paleotopographic estimations derived from stratigraphic and sedimentologic data.

The syn-rift period created extension that has been well studied but the lithospheric behaviour by flexure in the post-rift period has received little attention up to now. Assuming a two-layer extensional model, the Iberian Basin subsidence data show close relationship to the results of the partly lithospheric decoupled flexure model of Ter Voorde et al. (1998), where drowning by sediments of the rift shoulders take place only at the end of the flexure (post-rift) phase.

7. Comparison of derived stretching factors for the Iberian and Ebro Basins

A synthesis of the stretching factor values for these stages is summarised in Fig. 7. A close relationship is observed between crustal and subcrustal stretching factors, at the origin of both basins, subsidence styles and infill of sediments (Figs. 8, 12).

In the beginning, during the Autunian times (stage I, Fig. 12), both stretching factors are close to 1 (1.002 and 1.001) and δ is bigger than β. In stage II δ is bigger than β for all sections except for the Molina de Aragón section, with values of δ and β increasing in this stage relative to stage I. In stage III extension propagated from the SW to the NE with time, with values of δ and β also increasing in this period.

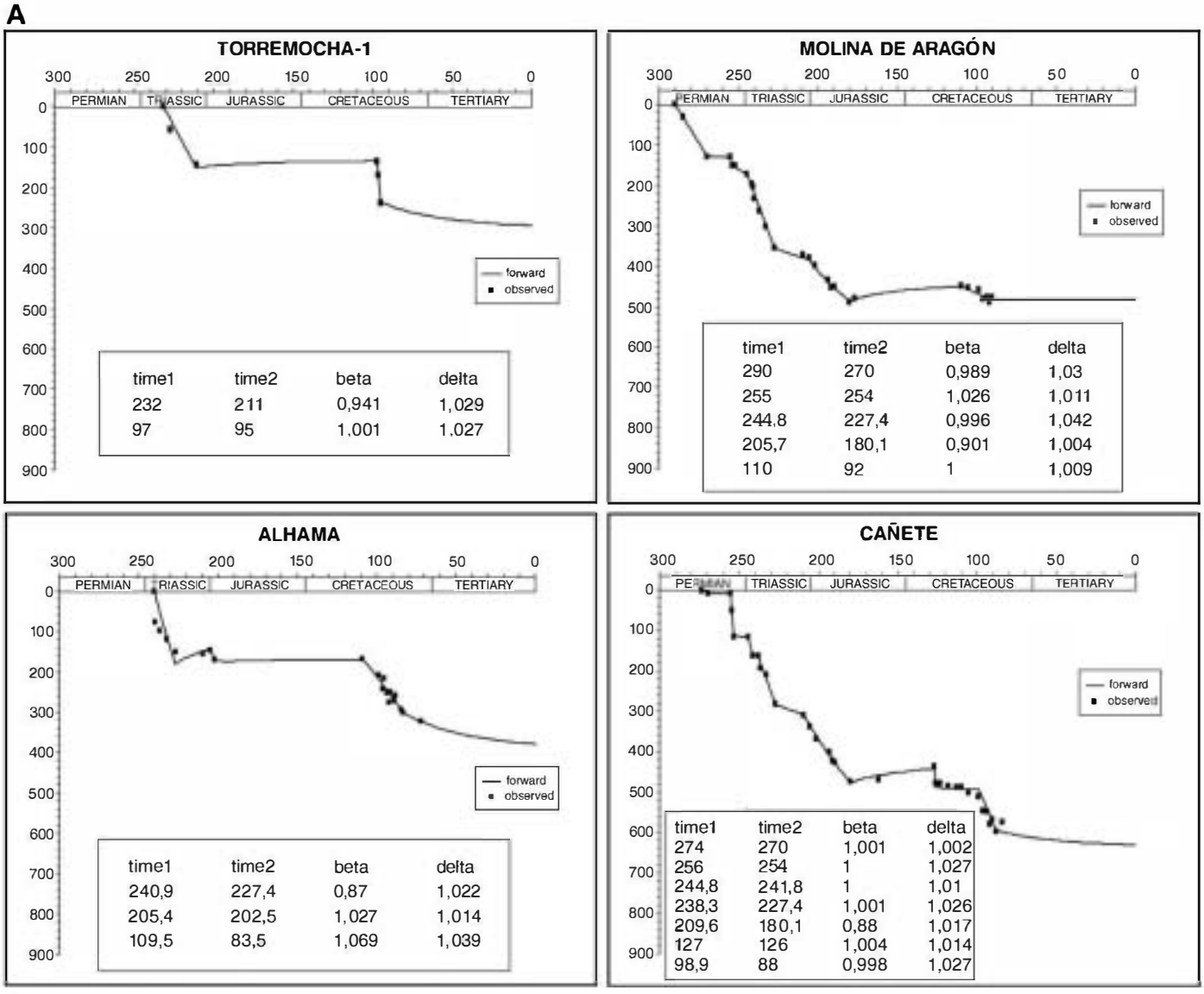

Fig. 10. A) Forward modelling curves and β and δ values for the defined phases for the Iberian Ranges. See Fig. 2B for the geographical locations. B) Continuation of A.

The latest analysed period (stage IV) shows an important change in the style of subsidence. In agreement with the increase in postrift subsidence, for the first time in its evolution the β factor is bigger than δ factor in one section of the Iberian Basin (Ter) and one well of the Ebro Basin (Buj-1). The beginning of a generalized heat conductive loss most likely explains this change.

8. Discussion

A total of five synrift phases (I to V, Fig. 7) have been observed in the study area. Phases I and II, of Permian age, only appear in the Iberian Basin, while phase IV only have been shown in the Ebro Basin. Phases III and V are observed simultaneously in both basins. An isolated phase related to local fault movements of the SW border of the Iberian Basin have been observed in Torremocha-1 well and cannot be correlated with phases in the central part of the basin.

The analysis of the subsidence and forward modelling shows that semigraben compartimentalisation explains better the major features of the origin and evolution of the Permian–Triassic Iberian and Ebro basins, as suggested earlier by Arche and López-Gómez (1996) and which is also supported by the asymmetric shape of the isopac maps for the Permian and Early Triassic sediments (Arche and López-Gómez, 1999a).

The forward modelling has been applied to the data using both one-layer and two-layer configurations in a systematic way and always the latter has provided the best fit between prediction and observation, especially in the Iberian Basin. These results clearly show that the basin formation mechanisms had a vertically heterogenous stretching effects ($\beta \neq \delta$), which may attributed partly by mantle heating and cooling effects, superimposed on stretching (cf. Van Wees et al., 1998), but also to simple-shear extension, related to major crustal fault zones as indicated in Fig. 8.

Some important consequences of simple-shear extension also explain aspects of the geometrical characteristics of the Iberian and Ebro basins. The prominent Paleozoic basement high that separates both basins until Ladinian times, the Ateca–Montalbán high (Fig. 8), can be interpreted as a hanging-wall central high as defined by Gibbs (1984, 1987), a zone without extension produced as active extension progrades away from the original fault, the original basin boundary fault becomes inactive, and the synthetic fault system to the NE was favored during Middle–Late Triassic extension. As total stretching for the Permian–Triassic period never exceeded 1.2, only a single generation of normal

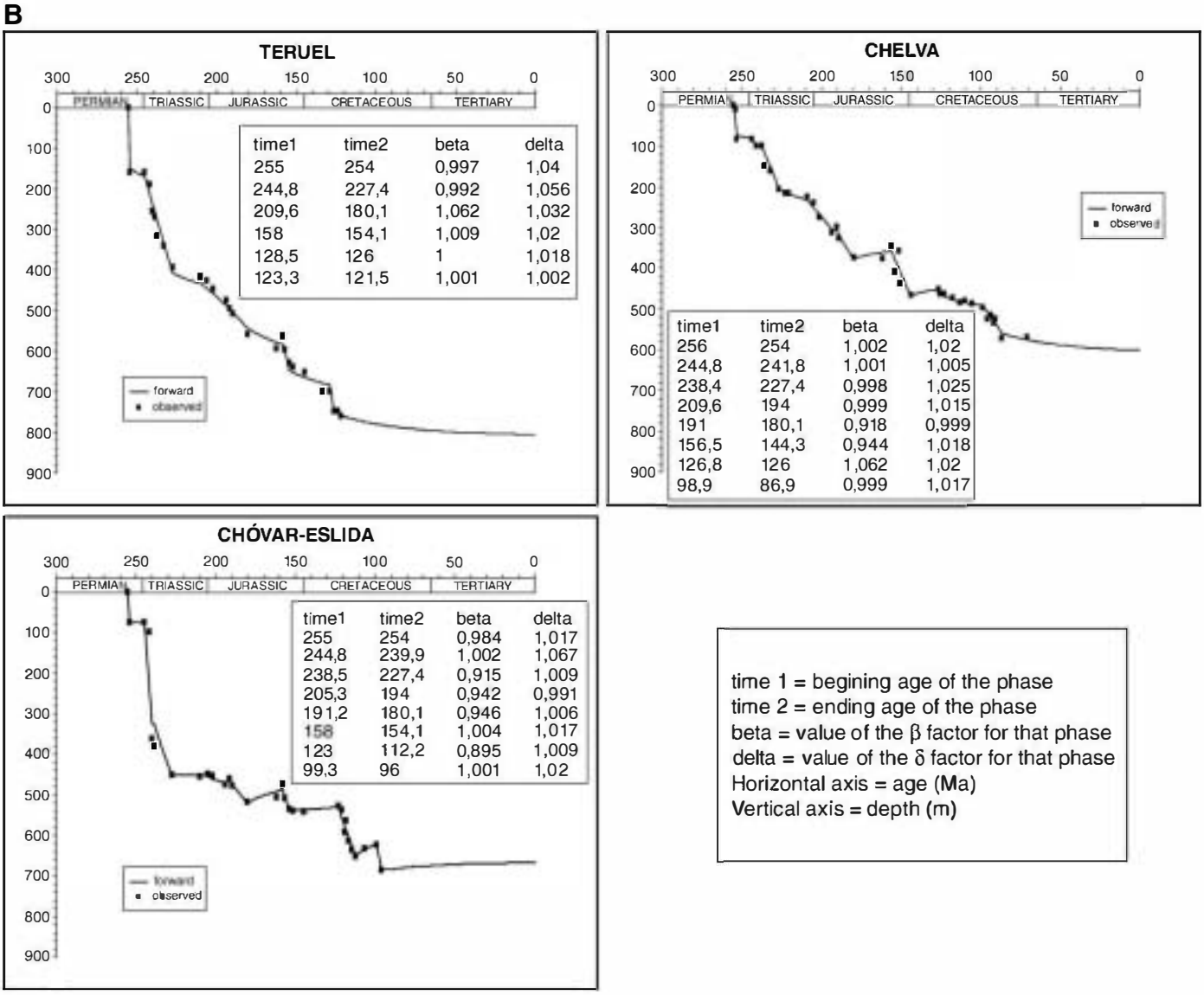

Fig. 10 (*continued*).

faults were developed and they did not flatten out totally in the hanging wall, nor a second fault system developed, as in some present-day western U.S.A. examples (Wernicke and Tilke, 1989).

A largely ignored interpretation of the aeromagnetic anomalies of the Iberian Ranges by Salas and Casas (1993) is that their NW–SE lineament correspond to a suture between two basement terranes with contrasting lithologic characteristics. Rey et al. (1998), using seismic profiles and gravity anomaly data, interpreted the SW part of this lineament as a denser body of metamorphic-granitic nature, than the counterpart to the NE of low metamorphic composition with a sharp contact in between.

The lithospheric structure under the Iberian Ranges shows some gently dipping reflectors (Banda et al., 1983), that reveal important lateral inhomogeneities in the lithospheric plate, a common feature of most of the Hercynian belt (McBride and England, 1994). These lineaments can be easily transformed in listric faults during extension, specially if the upward of the asthenosphere under the extensional area is asymmetric as in the case of the Baikal rift (Gao et al., 1994; Burov et al., 1994; Burov and Cloetingh, 1997).

A suture of contrasting continental blocks is found in the East African and Baikal rifts (Delvaux et al., 1995; Versfeld and Rosendahl, 1989) illustrating how the pre-rift structure of the basement and the lateral lithospheric inhomogeneities control the orientation of the rift architecture in the East African rift. In consequence, even if the Iberian Basin was created in response to strike-slip stress along the margins of the Iberian Plate (Arche and López-Gómez, 1996), the pre-existing weakness channelised the strain releasing it in a way similar to the cited present-day cases.

An important aspect of the results of the forward modelling, adopting simple shear extension, is that it seems highly contradictory in itself is that values of $\delta > 1$ are coeval with values of $\beta < 1$ in some periods (Fig. 12). How can compression in the lower lithosphere be coeval with extension in the upper lithosphere? Assuming a fully detached, two-layer lithospheric model, extension in the upper layer must be accomodated elsewhere, but not necessarily just underneath. This is the case in some present-day examples such as the Parentis Basin or the Viking Graben (Pinet and Colleta, 1990) or the West Shetland and West Fair Island basins (McBride and England, 1994), where stretching in the upper lithosphere coexists with compression in the lower lithosphere. A highly speculative explanation of the decoupling of deformation in the Iberian and Ebro Basins is that stretching by simple shear in contiguous basins such as Pyrenees or

Betics is accomodated in the deep parts of the Iberian Basin–Ebro Basin area (Puigdefábregas and Souquet, 1986). A more likely alternative explanation could be a lateral spreading of ductile lower crust during the propagation of the crustal detachment that caused the stretching in the Iberian and Ebro Basins, a mechanism described by McKenzie et al. (2000). The possible effects of intraplate-stress (Cloetingh, 1988; Cloetingh et al., 1985; Cloetingh and Kooi, 1992) remaind to be studied for the Permian–Triassic period in Central Iberia.

The above mentioned mechanisms can explain the modelled $\delta > 1$ are coeval with values of $\beta < 1$ in some periods. Nonetheless we believe that further study is required to prove this concept for the Iberian Ranges and Ebro Basin. In particular active mantle heating, in between the rifting stages (cf. Van Wees et al., 1998) can also well explain abnormally low and retarded postrift subsidence in the Iberian range. The emplacement of granites and eruption of andesitic rocks during the first and second phases of extension (Autunian and Thüringian) supports this. On the other hand, under these circumstances, the zone of coupling at the boundary between lithosphere and astenosphere is a zone of shear stress giving rise to high strain compressive zones just away from the astenosphere diapirs (Huismans et. al., 2001; Kennedy et al., 2002).

9. Conclusions

Quantitative subsidence analysis (backstripping method) and forward modelling of the extensional processes have been applied to the Permian–Triassic sediments of the Iberian and Ebro basins, using improved calculating programs, using a method that allows for infinite extensional phases, not for a limited number as in any other previous studies.

Improved analytical techniques have differentiated four synrift and one general postrift extensional phases in the Iberian Basin and three synrift and two postrift phases in the Ebro Basin; only two were identified prior to this study. Two of the synrift phases are common to both basins: the Scytian–Ladinian one and the Rhetian one.

The subsidence shows large differences along the basins, even if the phases are the same, ranging from 175 m–450 m of tectonic subsidence for the Permian–Triassic period in the Iberian Basin to 125 m–225 m for the Ebro Basin in the same period.

Crustal extension (δ) ranges from 0.997 to 1.155 in the Iberian Basin and from 0.985 to 1.075 in the Ebro Basin. Subcrustal (β) extension ranges from 0.828 to 1.027 in the Iberian Basin and from 0.838 to 1.028 in the Ebro Basin. These results are moderate in

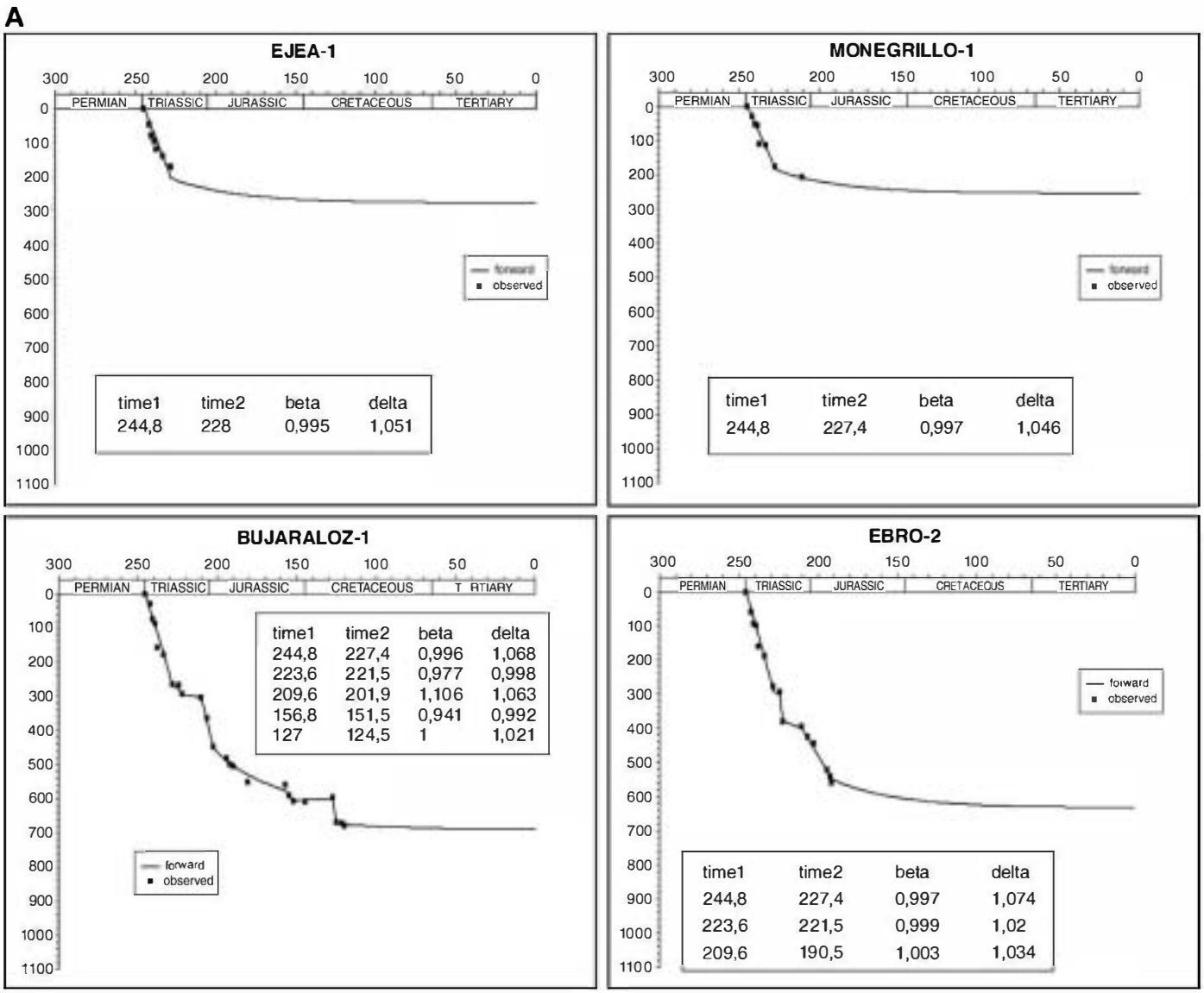

Fig. 11. A) Forward modelling curves and β and δ values for the defined phases for the Ebro Basin. See Fig. 2 B for the geographical locations. B) Continuation of A.

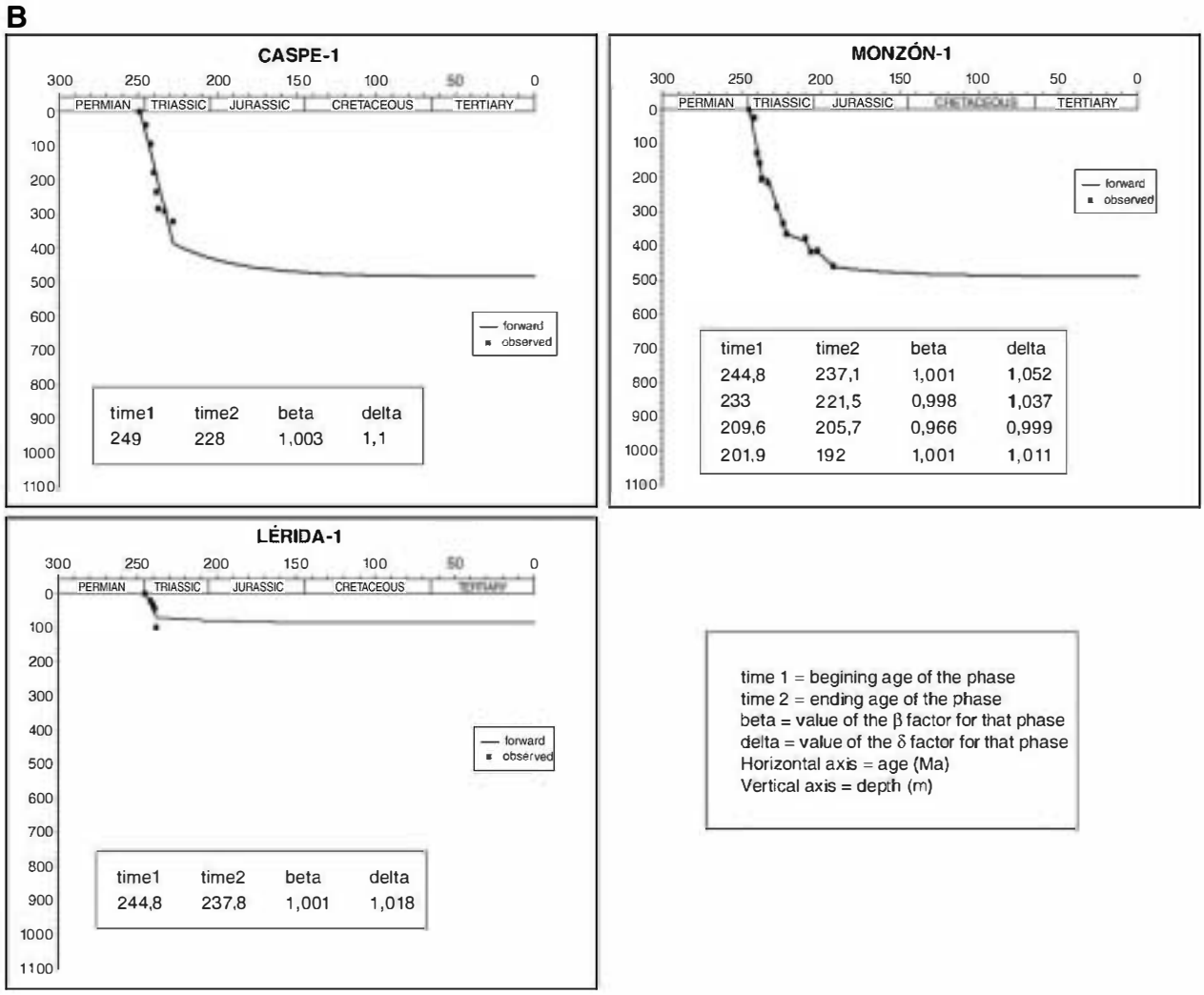

Fig. 11 (*continued*).

AUTUNIAN

	Torr-1	Mol	Alh	Ca	Ter	Chel	Ch-Esl	Ejea-1	Moneg-1	Buj-1	Ebro-2	Caspe-1	Monz-1	Lérida-1
δ	---	1.03	---	1.002	---	---	---	---	---	---	---	---	---	---
β	---	0.989	---	1.001	---	---	---	---	---	---	---	---	---	---

THÜRINGIAN

	Torr-1	Mol	Alh	Ca	Ter	Chel	Ch-Esl	Ejea-1	Moneg-1	Buj-1	Ebro-2	Caspe-1	Monz-1	Lérida-1
δ	---	1.011	---	1.027	1.04	1.02	1.017	---	---	---	---	---	---	---
β	---	1.026	---	1	0.997	1.002	0.984	---	---	---	---	---	---	---

SCYTIAN-LADINIAN

	Torr-1	Mol	Alh	Ca	Ter	Chel	Ch-Esl	Ejea-1	Moneg-1	Buj-1	Ebro-2	Caspe-1	Monz-1	Lérida-1
δ	---	1.042	1.022	1.01 / 1.026	1.056	1.005 / 1.025	1.067/ 1.009	1.051	1.046	1.068	1.074	1.1	1.052/ 1.037	1.018
β	---	0.996	0.87	1 / 1.001	0.992	1.001 / 0.998	1.002/ 0.915	0.995	0.997	0.996	0.997	1.003	1.001 / 0.998	1.001

RHAETIAN

	Torr-1	Mol	Alh	Ca	Ter	Chel	Ch-Esl	Ejea-1	Moneg-1	Buj-1	Ebro-2	Caspe-1	Monz-1	Lérida-1
δ	---	---	---	1.017	1.032	1.015	---	---	---	1.063	1.034	---	0.999	---
β	---	---	---	0.88	1.062	0.999	---	---	---	1.106	1.003	---	0.966	---

Fig. 12. β and δ stretching factors values for the Autunian, Thüringan, Scytian–ladinian and Rhaetian phases obtained from the studied sections and wells of both Iberian and Ebro Basins. See Fig. 2B for their location and Fig. 7 for the ages of the phases.

comparison to other classical extensional basins like the East African rifts or the Rhine Graben.

A two-layer extensional mechanism based on simple shear deformation offers the best fit between observational and calculated data.

It is necessary to study the whole of the NE Iberian Plate to explain how crustal extension in shallow lithospheric levels is compensated in depth by compression or different extensional rates in some zones, but this can only be elucidated by seismic reflection studies at lithospheric scales, beyond the scope of this work.

Acknowledgements

This is a contribution to Project CGL2005-01520/BTE and CGL2008-00093 (Spanish Ministry of Science and Technology) and to the Grupo de Análisis de Cuencas (UCM). This is a Netherlands Research School of Sedimentary Geology Publication NSG. The contributions of the two anonymous reviewers are acknowledged here because they have improved a previous version of this paper. Long discussions during the preparation of this paper with Mariano Marzo (U. Barcelona) are also acknowledged.

References

Álvaro, M., 1987. La subsidencia tectónica en la Cordillera Ibérica durante el Mesozoico. Geogaceta 3, 34–37.

Álvaro, M., Capote, R., Vegas, R., 1979. Un modelo para la evolución geotectónica de la Cordillera Celtibérica. Acta Geol. Hisp. 14, 172–177.

Arche, A., López-Gómez, J., 1989. Fluvial sedimentation during the early rifting phase in the Southeastern Iberian Ranges. 4th Int. Conf. Fluvial Sedimentology, Field Guide. Generalitat de Catalunya, Barcelona. 88 pp.

Arche, A., López-Gómez, J., 1996. Origin of the Permian–Triassic Iberian Basin, central-eastern Spain. Tectonophysics 266, 443–464.

Arche, A., López-Gómez, J., 1999a. Subsidence rates and fluvial architecture of rift-related Permian and Triassic alluvial sediments of the southeast Iberian Range, eastern Spain. Spec. Publs Int. Ass. Sediment. 28, 283–304.

Arche, A., López-Gómez, J., 1999b. Tectonic and geomorphic controls on the fluvial styles of the Eslida Formation, Middle Triassic, Eastern Spain. Tectonophysics 315, 187–207.

Arche, A., López-Gómez, J., Marzo, M., Vargas, H., 2004. The siliciclastics Permian–Triassic deposits in Central and Northeastern Iberian Peninsula (Iberian, Ebro and Catalan Basins): a proposal for correlation. Geologica Acta 2, 305–320.

Arche, A., Diez, J.B., López-Gómez, J., 2007. Identification of the Early Permian (Autunian) in the subsurface of the Ebro Basin, NE Spain, and its paleogeographic consequences. Journal of Iberian Geology, 33 (1), 125–133.

Arribas, J., 1985. Base litoestratigráfica de las facies Buntsandstein y Muschelkalk en la RamaAragonesa de la Cordillera Ibérica, zona Norte. Estudios Geológicos 41, 47–57.

Arribas, J., 1987. Las facies superiores del Muschelkalk en el borde de la Rama Aragonesa de la Cordillera Ibérica. Cuadernos de Geología Ibérica 11, 557–574.

Arribas, J., Marfil, R., De la Peña, J.A., 1985. Provenance of Triassic feldspatic sandstones in the Iberian Range (Spain): significance of quartz types. J. Sediment. Petrol. 55, 864–868.

Aurell, M., Bádenas, B., Bello, J., Delvene, G., Meléndez, G., Pérez-Urresti, I., Ramajo, J., 1999. El Calloviense y el Jurásico Superior en la Cordillera Ibérica Nororiental y la Zona de Enlace con la Cordillera Costero-Catalana en los sectores de Sierra de Arcos, Calanda y Xerta-Paüls. Cuadernos de Geología Ibérica 25, 73–110.

Banda, E., Udias, A., Mueller, S., Mezcua, J., Boloix, M., Gallart, J., Aparicio, A., 1983. Crustal structure beneath Spain from deep seismic sounding experiments. Phys. Earth Planet. Inter. 31, 277–280.

Bond, G., Kominz, M.A., 1984. Construction of tectonic subsidence curves for the Early Paleozoic miogeocline, southern Canadian Rocky Mountains: implications for subsidence mechanisms, age of break up and crustal thinning. Geol. Soc. Am. Bull. 95, 155–173.

Burov, E.B., Houdry, F., Diament, M., Déverchère, J., 1994. A broken plate beneath the North Baikal rift zone revealed by gravity modelling. Geophys. Res. Lett. 21, 2, 129–132.

Burov, E., Cloetingh, S., 1997. Thermomechanical effects of rift shoulder erosion on the evolution of extensional basins. Earth Planet. Sci. Lett. 150, 7–26.

Calvet, F., Marzo, M., 1994. El Triásico de las Cordilleras Costero Catalanas: estratigrafía, sedimentología y análisis secuencial. Field guide. III Coloquio de estratigrafía y Sedimentología del Triásico y Pérmico de España, pp. 1–53.

Canerot, J., 1982. Ibérica Central-Maestrazgo. In: García, A. (Ed.), Cretácico de España. Universidad Complutense de Madrid, pp. 273–344.

Chéry, J., Lucazeau, F., Daignières, M., Vilotte, J., 1992. Large uplift of rift flanks: a genetic link with lithospheric rigidity? Earth and planet. Sci. Lett. 112, 195–211.

Choukroune, P., 1989. The ECORS pyrenean deep seismic profile reflection data and the overall structure of an orogenic belt. Tectonics 8, 23–39.

Cloetingh, S., 1988. Intraplate stress, a new element in basin analysis. In: Kleinspehn, K., Paola, C. (Eds.), New perspectives in basin analysis. Springer, Berlin, pp. 305–330.

Cloetingh, S., Kooi, H., 1992. Intraplate stress and dynamic aspects of rift basins. Tectonophysics 215, 167–185.

Cloetingh, S., McQueen, H., Lambeck, K., 1985. On a tectonic mechanism for regional sea level variations. Earth Planet. Sci. Lett. 75, 157–166.

Cloetingh, S., van Wees, J.D., van der Beek, P.A., Spadini, G., 1995. Role of pre-rift rheology in kinematics of extensional basin formation: constrains from thermo-mechanical models of Mediterranean and intracratonic basins. Mar.Petrol. Geol. 12, 793–807.

De la Peña, J.A., Fonolla, F., Ramos, J.L., Marfil, R., 1977. Identificación del Autuniense en la Rama Aragonesa de la Cordillera Ibérica (provincia de Soria). Cuadernos de Geología Ibérica 4, 123–134.

Del Olmo, P., Olivé, A., Gutierrez, M., Aguilar, M., Leal, M., Portero, J.M., 1983. Memoria y mapa geológico de España. Escala 1:50.000, Serie Magna. 458, Paniza. Ministerio de Industria y Energía 1-80.

Delvaux, D., Moeys, R., Stapel, G., Melnikov, A., Ermikov, V., 1995. Paleostress reconstructions and geodynamics of the Baikal Rift region, Central Asia. Tectonophysics 252, 61–101.

Desegaulx, P., Moretti, I., 1988. Subsidence history of the Ebro Basin. J. Geodyn. 10, 9–24.

Díez, J.B., Grauvogel-Stamm, L., Broutin, J., Ferrer, J., Gisbert, J., Liñán, E., 1996. Première découverte d'une paléoflore anisienne dans le faciès "Buntsandstein" de la Branche Aragonaise de la Cordillère Ibérique (Espagne). C.R. Acad. des Sci. 323, 341–347 Paris.

Doubinger, J., López-Gómez, J., Arche, A., 1990. Pollen and spores from the Permian and Triassic sediments of the SE Iberian Ranges, Cueva de Hierro (Cuenca) to Chelva-Manzanera (Valencia-Teruel) region, Spain. Rev. Paleobot. Palynol. 66, 25–45.

ECORS Pyrenees Team, 1988. Deep reflection seismic survey across an entire orogenic belt: the ECORS Pyrenees profile. Nature 331, 508–511.

Gao, S., Davis, P.M., Liu, H., Slack, P.D., Logatchev, N., Kogan, M., Burkholder, P.D., Meyer, R.P., 1994. Asymmetric upward of the asthenosphere beneath the Baikal rift zone, Siberia. J. Geophys. Res. 99, 15319–15330.

Gaspar-Escribano, J.M., van Wees, J.D., ter Voorde, M., Cloetingh, S., Roca, E., Cabrera, L., Muñoz, J., Ziegler, P.A., García-Castellanos, D., 2001. Three-dimensional flexural modelling of the Ebro Basin (NE Iberia). Geophys. J. 145, 1–26.

Gawthorpe, R.L., Leeder, M.R., 2000. Tectonosedimentary evolution of active extensional basins. Basin Res. 12, 195–218.

Gueguen, E., Doglioni, C., Fernández, M., 1998. On the post-25 Mageodynamic evolution of the western Mediterranean. Tectonophysics 298, 259–269.

Gibbs, A.D., 1984. Structural evolution of extensional basin margins. J. Geol. Soc. London 141, 609–620.

Gibbs, A.D., 1987. Development of extension and mixed-mode sedimentary basins. Geol. Soc. Spec. Pub. 28, 19–33.

Gibbs, A.D., 1990. Linked fault families in basin formation. J. Struct. Geol. 12 (5/6), 795–803.

Gómez, J.J., 1978. El Jurásico en facies carbonatadas del Sector Levantino de la Cordillera Ibérica. Seminarios de Estratigrafía, vol. 4. 683 pp.

Gómez, J.J., Goy, A., 1979. Las unidades litoestratigráficas del Jurásico Medio y Superior en facies carbonatadas del Sector Levantino de la Cordillera Ibérica. Estudios Geológicos 35, 569–598.

Goy, A., Gómez, J.J., Yébenes, A., 1976. El Jurásico de la Rama Castellana de la Cordillera Ibérica (mitad norte): I. Unidades litoestratigráficas. Estudios Geológicos 32, 391–423.

Goy, A., Yébenes, A., 1977. Características, extensión y edad de la Formación Dolomías Tableadas de Imón. Cuadernos de Geología Ibérica 4, 375–384.

Gradstein, F.M., Agterberg, F.P., Ogg, J.G., Hardenbol, J., van Veen, P., Thierry, J., Huang, Z., 1995. Geochronology time scales and global stratigraphic correlation. SEPM Special Publication 54, 95–127.

Guimerá, J., Álvaro, M., 1990. Structure et évolution de la compression alpine dans la Chaîne Ibérique et la Chaîne Côtière Catalane (Espagne). Bull. Soc. Géol. Fr. 8 (VI), 339–348.

Huismans, R.S., Podladchikov, Y.Y., Cloetingh, S., 2001. Transition from passive to active rifting: relative importance of asthenospheric doming and passive extension of the lithosphere. J. Geophys. Res. 106, 11271–11291.

IGME, 1987. Contribución de la exploración petrolífera al conocimiento de la geología de España. Instituto Geológico y Minero de España, Madrid. 465 pp.

Jurado, M.J., 1989. El Triásico del subsuelo de la Cuenca del Ebro. Ph.D. Thesis. Departamento de Geología Dinámica, Geofísica y Paleontología, Universidad de Barcelona. 259 pp. Unpublished.

Jurado, M.J., 1990. El Triásico y Iásico basal evaporíticos del subsuelo de la cuenca del Ebro. In: Ortí, F., Salvany, J.M. (Eds.), Formaciones evaporíticas de la Cuenca del Ebro y cadenas periféricas y de la zona de Levante. Enresa, pp. 21–28.

Kennedy, L.A., Russell, J.K., Kopylova, M., 2002. Mantle shear zones revisited: the connection between the cratons and mantle dynamics. Geology 30, 419–422.

Kooi, H., Cloetingh, S., Burrus, J., 1992. Lithospheric necking and regional isostasy at extensional basins. 1. Subsidence and gravity modelling with an application to the Gulf of Lions margin (SE France). J. Geoph. Res. 97, 17553–17571.

Lago, M., Gil, A., Pocoví, J.A., Arranz, E., Galé, C., 2001. The Permian Calc-Alkaline magmatism of the Iberian belt (Spain): an update synthesis. Natura Bresciana 25, 181–188.

Leeder, M.R., Gawthorpe, R.L., 1987. Sedimentary models for extensional tilt block/half-graben basins. In: Coward, M.P., Dewey, J.F., Hancock, P.L. (Eds.), Continental extensional tectonics, vol. 28. Geological Society of London Special Publ., pp. 139–152.

Leeder, M.R., Collier, R.E., Abdul Haziz, L.H., Trout, M., Ferentinos, G., Papatheodorou, G., 2002. Tectono-sedimentary processes along an active marine/lacustrine half-graben margin, Alkionides Gulf, E. Gulf of Corinth, Greece. Basin Res. 14, 25–42.

López-Gómez, J., 1985. Sedimentología y estratigrafía de los materiales pérmicos y triásicos del sector SE de la Rama Castellana de la Cordillera Ibérica entre Cueva de

Hierro y Chelva (provincias de Cuenca y Valencia). Seminarios de Estratigrafía 11, 1–344.
López-Gómez, J., Arche, A., 1986. Estratigrafía del Pérmico y Triásico en facies Buntsandstein y Muschelkalk en el sector SE de la Rama Castellana de la Cordillera Ibérica. Estudios Geológicos 42, 259–270.
López-Gómez, J., Arche, A., 1992a. Las unidades litoestratigráficas del Pérmico y Triásico inferior y medio en el sector SE de la Cordillera Ibérica. Estudios Geológicos 48, 123–143.
López-Gómez, J., Arche, A., 1992b. Palaeogeographical significance of the Röt (Anisian, Triassic) Facies (Marines clays, muds and marls Fm.) in the Iberian Ranges, eastern Spain. Palaeogeo. Palaeoclimatol. Palaeoecol. 91, 347–361.
López-Gómez, J., Arche, A., 1993a. Sequence stratigraphic analysis and palaeogeographic interpretation of the Buntsandstein and Muschelkalk facies (Permo-Triassic) in the SE Iberian Range, E Spain. Palaeogeo. Palaeoclimatol. Palaeoecol. 103, 179–201.
López-Gómez, J., Arche, A., 1993b. Arquitecture of the Cañizar fluvial sheet sandstones, Early Triassic, Iberian Ranges, eastern Spain. Spec. Publs Int. Ass. Sediment. 17, 363–381.
López-Gómez, J., Arche, A., 1994. La Formación Brechas de Tabarreña (Pérmico Inferior): depósitos de flujos con densidad variable al SE de la Cordillera Ibérica, España. Bol. R. Soc. Esp. Hist. Nat. (Sec. Geol.) 89 (1–4), 131–144.
López-Gómez, J., Arche, A., 1995. El Pérmico y el Triásico del Levante español. Características principales y consideraciones paleogeográficas. Cuadernos de Geología Ibérica 19, 201–234.
López-Gómez, J., Arche, A., 1997. The Upper Permian boniches conglomerates formation: evolution from alluvial fan to fluvial system environments and accompanying tectonic and climatic controls in the southeast Iberian Ranges, central Spain. Sed. Geology 114, 267–294.
López-Gómez, J., Arche, A., Calvet, F., Goy, A., 1998. Epicontinental marine carbonate sediments of the Middle and Upper Triassic in the westernmost part of the Tethys Sea, Iberian Peninsula. In: Bachmann, G.H., Lerche, I. (Eds.), Epicontinental Triassic, Zentralb. für Geol. und Paläontol., I, vol. 9–10, pp. 1033–1084.
López-Gómez, J., Arche, A., Pérez-López, A., 2002. In: Gibbon, W., Moreno, T. (Eds.), Permian and Triassic. Geology of Spain. Geol. Soc., London. 185-212 pp.
López-Gómez, J., Más, R., Arche, A., 1993. The evolution of the Middle Triassic (Muschelkalk) carbonate ramp in the SE Iberian Ranges, eastern Spain: sequence stratigraphy, dolomitization processes and dynamic controls. Sed. Geology 87, 165–193.
Mas, J.R., 1981. El Cretácico inferior de la región noroccidental de la provincia de Valencia. Seminarios de Estratigrafía 8, 1–408.
McBride, J.H., England, R.W., 1994. Deep seismic reflection structure of the Caledonian orogenic front west of Shetland. J. Geol. Soc. London 151, 9–16.
McKenzie, D., 1978. Some remarks on the development of sedimentary basins. Earth and Planet. Sci. Lett. 40, 25–32.
McKenzie, D., Nimmo, F., Jackson, J.A., 2000. Characteristics and consequences offlowin the lower crust. J. Geoph. Res. 105, 11029–11046.
Meléndez, N., 1983. El Cretácico de la región de Cañete-Rincón de Ademuz (provincias de Cuenca y Valencia). Seminarios de Estratigrafía 9, 1–242.
Meléndez, G., Aurell, M., Atrops, F., 1990. Las unidades del Jurásico Superior en el sector nororiental de la Cordillera Ibérica: nuevas subdivisiones litoestratigráficas. Cuadernos de Geología Ibérica 14, 225–245.
Meléndez, A., Aurell, M., Bádenas, B., Soria, A.R., 1995a. Las rampas carbonatadas del Triásico Medio en el sector central de la Cordillera Ibérica. Cuadernos de Geología Ibérica 19, 173–199.
Meléndez, A., Aurell, M., Bádenas, B., Soria, A., 1995b. Las rampas carbonatadas del Triásico Medio en el sector central de la Cordillera Ibérica. Cuadernos Geología España 19, 173–200.
Monrose, H. 1968. Reconnaisance geologique de la region de Reznos (Saragosse), Espagne. Thèse du Licenciature, Universitê du Bordeaux.
Morgan, P., Fernández, M., 1992. Neogene vertical movements and constraints on extension in the Catalan Coastal Ranges, Iberian Peninsula, and the Valencia Trough (western Mediterranean). Tectonophysics 203, 185–201.
Morley, C.K., 1999. Boundary fault angle with particular reference to the Lokichar fault, Turkana region, Kenya. In: Morley, C.K. (Ed.), Geoscience of Rift Systems-Evolution of East Africa. AAPG Studies in Geology, vol. 44, pp. 115–130.
Muñoz, J.A., 1992. Evolution of a continental collision belt: ECORS-Pyrenees crustal balanced cross-section. In: McClay, K.R. (Ed.), Thrusts Tectonics. Chapman and Hall, London, pp. 235–246.
Muñoz, A., Ramos, A., Sopeña, A., Sánchez-Moya, Y., 1995. Caracterización de las Unidades Litoestratigráficas del Triásico en el subsuelo del tercio noroccidental de la Cordillera Ibérica y áreas adyacentes. Cuadernos de Geología Ibérica 19, 129–171.
Ortí, F., 1974. El Keuper del Levante Español. Estudios Geológicos 30, 7–46.
Ortí, F., 1987. Aspectos sedimentológicos de las evaporitas del Triásico y del Liásico inferior en el E de la Península Ibérica. Cuadernos de Geología Ibérica 11, 873-858.
Ortí, F., 1990. Introducción a las evaporitas de la Cuenca Terciaria del Ebro. In: Ortí, F., Salvany, J. (Eds.), Formaciones evaporíticas de la cuenca del Ebro y cadenas periféricas, y de la zona de Levante. Enresa, GPPG, Barcelona, pp. 62–66.
Pérez-Arlucea, M., Sopeña, A., 1985. Estratigrafía del Pérmico y Triásico en el sector central de la Rama Castellana de la Cordillera Ibérica (provincias de Guadalajara y Teruel). Estudios Geológicos 41, 207–222.
Pinet, B., Colleta, B., 1990. Probing into extensional basins: comparison of recent data and derivation of tentative models. Tectonophysics 173, 185–197.
Puigdefábregas, C., Souquet, P., 1986. Tectonosedimentarycycles and depositional sequences of the Mesozoic and Tertiary from the Pyrenees. Tectonophysics 129, 173–203.
Puigdefábregas, C., Muñoz, J.A., Marzo, M., 1986. Thrust belt development in the eastern Pyrenees and related depositional sequences in the southern foreland basin. Spec. Publ. Int. Assoc. Sedimentol. 8, 229–246.
Ramos, A., 1979. Estratigrafía y Paleogeografía del Pérmico y Triásico al oeste de Molina de Aragón (provincia de Guadalajara). Seminarios de Estratigrafía 6, 1–313.
Rey, C., Tejero, R., Gómez-Ortíz, D., 1998. Estudio de la Cuenca de Almazán a partir de datos geofísicos. Geogaceta 24, 259–262.
Rey, D., Ramos, A., 1991. Estratigrafía y sedimentología del Pérmico y Triásico del sector Deza-Castejón (Soria). Rev. Soc. Geol. España 4, 105–125.
Rey, D., Turner, P., Yalif, Y., 1988. Paleomagnetism and Magnetostratigraphy of the Triassic rocks of the Iberian Ranges, Spain. J. Geol. Soc. London 146, 61–76.
Riba, O., Reguant, S., Villena, J., 1983. Ensayo de síntesis estratigráfica y evolutiva de la cuenca terciaria del Ebro. Libro Jubilar J.M. Ríos. Geología de España II. IGME, Madrid, pp. 131–159.
Roca, E., Guimerá, J., Salas, R., 2001. Mesozoic extensional tectonics in the Southern Iberian Chain. Geol. Mag. 131, 155–168.
Roca, E., Frizon de Lamotte, D., Mauffret, A., Bracène, R., Vergés, J., Benaouali, N., Fernández, M., Muñoz, A., Zeyen, H., 2004. TRANSMED-TRANSECT II: a desription of the section and of the data sources. In: Cavazza, W., Roure, F., Spackman, W., Stampfli, G.M., Ziegler, P. (Eds.), CD of the Mediterranean Consortium for the 32nd International Geological Cogress. Springer Verlag, Berlin.
Roest, W.R., Srivastava, S.P., 1991. Kinematics of the plate boundaries between Eurasia, Iberia and Africa in the North Atlantic from the late Cretaceous to present. Geology 19, 613–616.
Roure, F., Choukroune, P., ECORS Pyrenees Team, 1989. ECORS deep seismic data and balanced cross sections: geometric constraints on the evolution of the Pyrenees. Tectonics 8, 41–50.
Royden, L., Keen, C.E., 1980. Rifting process and thermal evolution of the continental margin of eastern Canada determined from subsidence curves. Earth Planet. Sci. Lett. 51, 343–361.
Sacher, L., 1966. Stratigraphie unf Tektonik der Norwestlichen Hesperischen ketten bei Molina de Aragón (Spanien). Teil 1. Stratigraphie (Palaozoikum). N. J. Geol. Und Palaont. 124 (2), 151–167.
Salas, R., 1989. Evolución estratigráfica secuencial y tipos de plataformas de carbonatos del intervalo Oxfordiense-Berriasiense en las cordilleras ibérica oriental y costero catalana meridional. Cuadernos de Geología Ibérica 13, 121–157.
Salas, R., Guimera, J., Mas, R., Martín-Closas, C., Meléndez, A., Alonso, A., 2001. Evolution of the Mesozoic Central Iberian Rift System and its cainozoic inversion (Iberian Chain). In: Ziegler, P.A., Cavazza, W., Robertson, A.H.F., Crasquin-Soleau, S. (Eds.), Peri-Thetys Memoir 6: Peri-Thetyan Rift/Wrench Basins and Passive Margins. Mem. Mus. Nac. Hist. Nat., vol. 186, pp. 145–185.
Salas, R., Casas, A., 1993. Mesozoic extensional tectonics, stratigraphy and crustal evolution during the Alpine cycle of the eastern Iberian basin. Tectonophysics 228, 33–55.
Salvany, J.M., 1990. Introducción a las evaporitas triásicas de las cadenas periféricas de la Cuenca del Ebro: Catalánides, Pirineo y región Cantábrica. In: Ortí, F., Salvany, J.M. (Eds.), Formaciones evaporíticas de la Cuenca del Ebro y cadenas periféricas y de la zona de Levante. Enresa, pp. 9–20.
Sclater, J.G., Christie, P.A.F., 1980. Continental stretching: an explanation of the post Mid-Cretaceous subsidence of the central North Sea basin. J. Geoph. Res. 85, 3711–3739.
Sopeña, A., Doubinger, J., Ramos, A., Pérez-Arlucea, M., 1995. Palynologie du Permian et du Trias dans le centre de la Péninsule Ibérique. Sci. Geol. Bull. 48, 119–157.
Sopeña, A., López-Gómez, J., Arche, A., Pérez-Arlucea, M., Ramos, A., Virgili, C., Hernando, S., 1988. Permian and Triassic Rift basins of the Iberian Peninsula. In: Manspeizer, W. (Ed.), Triassic-Jurassic Rifting. Continental Breakup and the Origin of the Atlantic Ocean and Passive Margins. Elsevier, Amsterdam, pp. 757–786.
Srivastava, S.P., Roest, W.R., Kovacs, L.C., Oakey, G., Lévesque, S., Verhoef, J., Macnab, R., 1990. Motion of Iberia since the Late Jurassic: results from detailed aeromagnetic measurements in the Newfoundland basin. Tectonophysics 184, 229–260.
Stapel, G., Cloetingh, S., Pronk, B., 1996. Quantitative subsidence analysis of the Mesozoic evolution of the Lusitanian basin (western Iberian margin). Tectonophysics 266, 493–507.
Steckler, M.S., Watts, A.B., 1978. Subsidence of the Atlantic-type continental margin off New York. Earth Planet. Sci. Lett. 41, 1–13.
Torres, T., 1990. Primeros resultados de una datación palinológica en el Keuper de la Rama Castellana de la Cordillera Ibérica y el Subbético frontal. In: Ortí, F., Salvany, J. (Eds.), Formaciones evaporíticas de la cuenca del Ebro y cadenas periféricas, y de la zona de Levante. Enresa, GPPG, Barcelona, pp. 19–223.
Ter Voorde, M., van Balen, R.T., Bertotti, G., Cloetingh, S., 1998. The influence of a stratified rheology on the flexural response of the lithosphere to (un)loading by extensional faulting. Geophys. J. Int. 134, 721–735.
Van der Beek, P., Cloetingh, S., Andriassen, P., 1994. Mechanisms of extensional basin formation and vertical motions at rift flanks: constraints from tectonic modelling and fission-track thermocronology. Earth Planet. Sci. Lett. 121, 417–433.
Van Wees, J.D., Cloetingh, S., 1994. A finite difference technique to incorporate spatial variations in rigidity and planar faults into 3-D models for lithospheric flexure. Geophys. J. Int. 117, 179–195.
Van Wees, J.D., Arche, A., Beijdorff, C.G., López-Gómez, J., Cloetingh, S.A.P.L., 1998. Temporal and spatial variations in tectonic subsidence in the Iberian Basin (eastern Spain): inferences from automated forward modelling of high-resolution stratigraphy (Permian–Mesozoic). Tectonophysics 300, 285–310.
Van Wees, J.D., Stephenson, R.A., 1995. Quantitative modelling of basin and rheological evolution of the Iberian Basin (Central Spain): implications for lithospheric dynamics of intraplate extension and inversion. Tectonophysics 252, 163–178.
Van Wees, J.D., Stephenson, R.A., Stovba, S.M., Shymanovskyi, V.A., 1996. Tectonic variation in the Dniepr-Donets Basin from automated modelling of backstripped subsidence curves. Tectonophysics 268, 257–280.
Van Wees, J.D., Beekman, F., 2000. Lithosphere reology during intraplate basin extension and inversion. Inferences from automated modelling of four basins in western Europe. Tectonophysics 300, 219–242.

Vegas, R., Banda, E., 1982. Tectonic framework and Alpine evolution of the Iberian Peninsula. Earth Evolution Sci. 4, 320–343.

Versfeld, J., Rosendalh, B.R., 1989. Relationship between pre-rift structure and rift architecture in Lakes Tanganika and Malawi. Nature 337, 354–357.

Vergés, J., García-Senz, J.M., 2001. Mesozoic evolution and Cenozoic inversión of the Pyrenean Rift. In: Ziegler, P., Cavazza, W., Robertson, A.H.F., Crasquin-Soleau, S. (Eds.), Peri-Tethys Memoir 6: Pery-Tethyan Rift/Wrench Basins and Passive Margins. Mémoires Muséum National d'Histore Naturelle, voL 186, pp. 187–212. Paris.

Vergés,J., Fernàndez, M., Martínez, A., 2002. The Pyrenean orogen: pre-, syn-, and post-collisional evolution. In: Rosenbaum, J.G., Lister, G.S. (Eds.), Reconstruction of the evolution of the Alpine-Himalayan Orogen. J. Virt. Explorer, voL 8, pp. 55–84.

Vilas, L., Mas, R., García, A., Arias, C., Alonso, A., Meléndez, N., Rincón, R., 1982. Ibérica SuroccidentaL In: García, A. (Ed.), Cretácico de España. Universidad Complutense de Madrid, pp. 457–513.

Wernicke, B., Tilke, P., 1989. Extensional tectonic framework of the U.S. Central Atlantic Passive Margin. In: Tankard, A., Balkwill, H.R. (Eds.), Extensional tectonics and stratigraphy of the northern Atlantic margins. AAPG, voL 46, pp. 7–21.

Young, M.J., Gawthorpe, R.L., Sharp, LR., 2002. Architecture and evolution of syn-rift clastic depositional systems towards the tip of a major fault segment, Suez Rift, Egypt. Basin Res 14, 1–24.

Ziegler, P.A., 1988. Post-Hercynian plate reorganization in the Tethys and Artic-North Atlantic domains. In: Manspeizer, W. (Ed.), Triassic-Jurassic rifting. Continental Breakup and teh Origin of the Atlantic Ocean and Passive Margins. . Developments in Geotectonics, vol. 22B. Elsevier, Amsterdam, pp. 711–755.

Zoetemeijer, R., Desegaulx, P., Cloetingh, S., Roure, F., Moretti, I., 1990. Lithospheric dynamics and tectonic-stratigraphic evolution of the Ebro Basin. J. Geophys. Res. 95 (B3), 2701–2711.